Title
POWER REQUIREMENTS FOR MIXING OF LIQUID-GAS SYSTEMS

Authors
Clark, Michael Wayne
Vermeulen, Theodore.

Publication Date
1963-08-30

UCRL-10996

University of California

Ernest O. Lawrence Radiation Laboratory

POWER REQUIREMENTS FOR MIXING OF LIQUID-GAS SYSTEMS

DISCLAIMER

Research and Development

UCRL-10996
UC-37 Instruments
TID-4500 (19th Ed.)

UNIVERSITY OF CALIFORNIA
Lawrence Radiation Laboratory
Berkeley, California

Contract No. W-7405-eng-48

POWER REQUIREMENTS FOR MIXING OF LIQUID-GAS SYSTEMS

Michael Wayne Clark and Theodore Vermeulen

August 30, 1963

Printed in USA. Price $1.50. Available from the
Office of Technical Services
U. S. Department of Commerce
Washington 25, D.C.

POWER REQUIREMENTS FOR MIXING OF LIQUID-GAS SYSTEMS

Contents

POWER REQUIREMENTS FOR MIXING OF LIQUID-GAS SYSTEMS

Michael Wayne Clark and Theodore Vermeulen

Lawrence Radiation Laboratory and Department of Chemical Engineering
University of California, Berkeley, California

August 30, 1963

ABSTRACT

The power requirements of agitated liquid-gas systems using both four-bladed flat-paddle impellers and a four-bladed turbine in a baffled cylindrical tank have been investigated. The power-number reduction has been related qualitatively to cavitation, and is correlated as a function of Weber number, geometrical factors, and the volumetric gas holdup. The gas holdup has been found to vary with impeller speed and impeller dimensions, as well as gas flow rate and liquid properties.

Incipient vortex formation, whereby air is introduced downward into an agitated liquid, was encountered and investigated. A correlation involving geometrical factors and the Froude number was developed to predict the onset of this phenomenon and the subsequent power-number behavior.

INTRODUCTION

Gas absorption, either to bring about a reaction or to dissolve a gas in a liquid, is a very common unit operation. The types of equipment used for this work fall into three general groups: (a) towers, (b) scrubbers, and (c) mechanical agitators within a container. In selecting the most suitable equipment for a particular gas absorption the following factors are important: the relative quantities of gas and liquid, and the amount of solids present or formed during the reaction.

In general, mechanical agitation is favored if the amount of liquid is large compared with the gas flow rate, and any solids are present in the system. An example of such an industrial situation is the hydrogenation of unsaturated fatty oils, or the production of penicillin. A mechanically agitated vessel is also needed when the reaction is conducted in a batch operation with respect to the liquid.

In view of the numerous applications of liquid-gas agitators, and liquid-liquid and single-liquid agitated contactors as well, a considerable body of literature has been developed in these areas.

Agitation of Single-Phase Liquid Systems

The agitation behavior of a homogeneous liquid phase provides a good starting point for developing information on two-phase systems.

Very early in the published literature on mixing-power requirements, we find the introduction of dimensionless variables to describe system behavior. White and co-workers[24] used paddle-type impellers in unbaffled tanks, and presented their data for power consumption, P, in the form

$$P = k\, L^a\, N^b\, \mu^c\, \rho^d\, T^e\, W^f\, H^g, \qquad (1)$$

where P is the power input to the system, L the impeller diameter, N the impeller speed, μ the fluid viscosity, ρ the fluid density, T the tank diameter, W the impeller width, and H the tank height. Later experimenters have rearranged these results, and their own, in terms of a dimensionless power number, P_0:

$$P_0 = Pg_c / N^3 L^5 \rho . \qquad (2)$$

As work was extended into baffled tanks in the turbulent-flow region, it was generally found that the power number remained constant over a wide range of variation of the Reynolds number, although this constant differed for the various geometrical systems investigated. In order to minimize this variation of P_0 with the geometrical parameters, an alternative known form of the power number, $P_w = Pg_c / N^3 L^4 W \rho$, can be utilized.

Agitation of Two-Phase Immiscible Systems

The next step in the investigation of agitated systems was to look at the problem of liquid-liquid contacting, a process that is widely used in various extraction processes. Rea and Vermeulen[16] extended the above type of investigation into the two-phase region, working in both baffled and unbaffled tanks. They correlated their results in terms of the same dimensionless variables, relating impeller speed and geometry to fluid properties such as mean density and viscosity for the mixtures. Since the second phase in these studies was still an incompressible liquid, the correlations did not differ greatly from those for single-phase liquid studies.

An important addition to the experimental data on two-phase systems was the use of photoelectric techniques to determine the bubble sizes in agitated vessels. Langlois[11,21], Rea and Vermeulen[16], Fick[7], Calderbank[3,4], and Rodger, Trice, and Rushton[17] used various modifications of this system to investigate a variety of tank and impeller geometries, as well as pertinent fluid variables and impeller speed. These studies indicated that there was a large variation of droplet size with position in the mixing vessel, the droplets being smaller near the impeller and increasing rapidly in size as the probe was moved away from the impeller region. Fick, and later Vanderveen,[20] found that this was due to the rate of coalescence of the discontinuous phase, and that an important variable was the interfacial tension between the two

fluids. A later report by Weiss, Fick, Houston, and Vermeulen[22] gives a comprehensive overall picture of dispersed-phase distribution patterns in liquid-liquid agitation.

In extending this work to gas-liquid systems, Williams[25] pointed out that very small amounts of surface contaminants could have a large effect upon the bubble size in such systems, a factor which is verified by observations he cites and by the theoretical treatment in a recent book by Levich.[12]

Hydrodynamics of Two-Phase Bubble Stability

Theoretical approaches valuable in the area of bubble stability and breakup are reviewed by Hinze[9] and Levich.[12] Through order-of-magnitude estimates of the various force terms, these authors are able to show the significance of important dimensionless groups such as the Weber number, Reynolds number, and viscosity ratio. Unfortunately the complexity of the Navier-Stokes equations, coupled with the force balances on the bubbles which are of indefinite geometrical shape, makes the solution to the equations very difficult even for the simplest types of boundary conditions.

The condition for bubble breakup is usually given as the point where the dynamic pressure, $\rho U^2/2$, of the medium exceeds the capillary pressure, σ/R, with U the mean relative velocity between the bubble surface and the surrounding liquid bulk. Levich[12] shows that this does not appear to hold true for the rising of large (unstable) gas bubbles, and proposes the following mechanism for bubble break up: "The drag exerted by the liquid sets the gas inside into motion. This motion, being rotational or possibly turbulent in nature, creates a dynamic pressure $\rho' U'^2/2$ within the bubble, (with U' being the velocity within the bubble relative to the bubble surface, and ρ' being the gas density). If this dynamic pressure exceeds the capillary forces holding the bubble together, the bubble must inevitably break up."

Levich then develops an expression for a critical bubble radius,

$$a_{cr} = (\text{const}) \frac{\sigma}{U^2 (\rho')^{1/3} \rho^{2/3}} \quad . \qquad (3)$$

Unfortunately this expression is difficult to apply, the value of U being usually unknown in an agitated system. In addition, if the flow of the outer fluid is in the turbulent region, the mechanism of bubble breakup becomes dependent mainly upon the localized velocity fluctuations in the fluid. This mechanism of bubble breakup is discussed in qualitative terms by Hinze.[10] An eventual solution to the problem may perhaps be found in the current statistical treatments of turbulent flow.

Agitation of Gas-Liquid Mixtures

There have been three main areas of investigation into gas-liquid agitation, i.e., power input into the system, sizes of bubbles existing in the system, and mass-transfer behavior between the gas and liquid phases.

Most of the mass-transfer work has been done with the sulfite oxidation system.[5,26,15,23] Cooper, Fernstrom, and Miller, in an early investigation using vaned-disk impellers and the sulfite-oxidation system, indicated that the volumetric absorption coefficient varied with (agitator power)$^{0.5}$ and with (gas velocity)$^{0.67}$. The method of gas introduction was from a single orifice beneath the impeller center. More recent work by Yoshida et al.[26] gives values of $k_G a$ and $k_L a$ versus impeller rpm. Phillips and Johnson[15] have given evidence that neither gas- nor liquid-side resistance completely controls the oxygen transfer rate, but that there is a complicated interrelation of variables.

The major contributions to the field of bubble-size determination have come from the same photoelectric technique applied in the liquid-liquid work. Although these authors[4,16,21] give a good first estimate as to the size of bubbles that will exist under a given flow condition, their results (which exhibit a large amount of experimental scatter) do not explain the mechanisms that determine the bubble size.

Work relative to the power required to achieve a gas-liquid dispersion is rather limited. Although several investigators have

measured power requirements, little effort has been made to explain the large reduction in power that occurs when gas is introduced into the agitated system. Oyama and Endoh[14] correlated P/P^* against the dimensionless group Q_g/ND^3, where P is the power input to the liquid-gas system, P^* is the power input to the pure liquid under the same agitation conditions, Q_g is the volumetric gas flow rate, N the impeller speed, and D the impeller diameter (L). Hyman[10] gives an average value of this correlation obtained from several authors, but indicates that the exact form of the curve can vary slightly with impeller design. Oyama and Aiba[14] have indicated the possible qualitative effects of system geometry, but they do not give a final correlation involving either the gas flow rate or gas holdup.

STATEMENT OF THE PROBLEM

The mechanism of power dissipation and that of bubble breakup are closely related in agitated two-phase systems. The power consumption should therefore furnish the key to the mass-transfer and interfacial-area behavior in such systems. Thus, since the power is itself a dependent variable, a suitable correlation of the power requirements in liquid-gas mixing should be an aid in establishing better knowledge of what is occurring in these systems. Also such a correlation would be valuable in the design of agitation equipment. The reduction in power that accompanies the introduction of the gas phase is difficult to explain in terms of the actual physical situation, and at present there is no explanation of the phenomenon.

The purpose of this work has been to investigate and to correlate the pertinent variables of the power input to an agitated liquid system into which a gas is sparged from below. The power reduction that occurs has been related to cavitation as a possible explanation of what is occurring physically. In addition, the gas holdup has been investigated as a function of gas rate and impeller speed. A third area of study was encountered when mixing was sufficiently intense to introduce air downward from the upper liquid surface into the agitated liquid; this incipient vortex formation has been explored experimentally and correlated.

EXPERIMENTAL PROGRAM

Equipment

The mixing vessel used in the experimental program was a stainless steel tank of 10.0 inches internal diameter, shown in Fig. 1. The tank was fitted with 1/4-in.-o.d. copper coils for circulation of cooling water, soldered to the outside surface. The 1/8-in. aluminum bottom plate was drilled with 25 holes of 1/32-in. diameter on a 1-in.-square grid; this configuration was chosen to make the liquid-gas mixture as uniform as possible after initial introduction of the gas phase. The bottom plate was gasketed on both sides, so that it could be removed and solid plates inserted to obtain reference data for the pure liquid. The tank was equipped with four 1-in.-wide baffles extending the full height of the tank, and spaced at 90° intervals around the tank wall. The impellers used were constructed entirely of stainless steel; the dimensions are shown in Table I.

In order to measure the power to the system, the tank was suspended from its cover, and this in turn was attached to the channel-iron frame through a mercury-sealed thrust bearing. This construction allowed free rotation of the tank, for measuring the applied torque by means of a pulley and a series of suspended weights. The force required was measured by means of a 20-lb-capacity pan balance with a 2-lb scale accurate to within 0.01 lb. An electric microswitch and counter were used to measure actual impeller rpm.

The impellers were driven by a V-belt drive connected to a 3/4-horsepower 3-phase 60-cycle 220-volt 216-rpm right-angle gear motor supplied by Electra Motors, Inc. Step-cone pulleys were mounted on the motor shaft and above the tank top, allowing the impellers to run at fixed speeds of 96, 132, 156, 199, 246, 300, and 396 rpm.

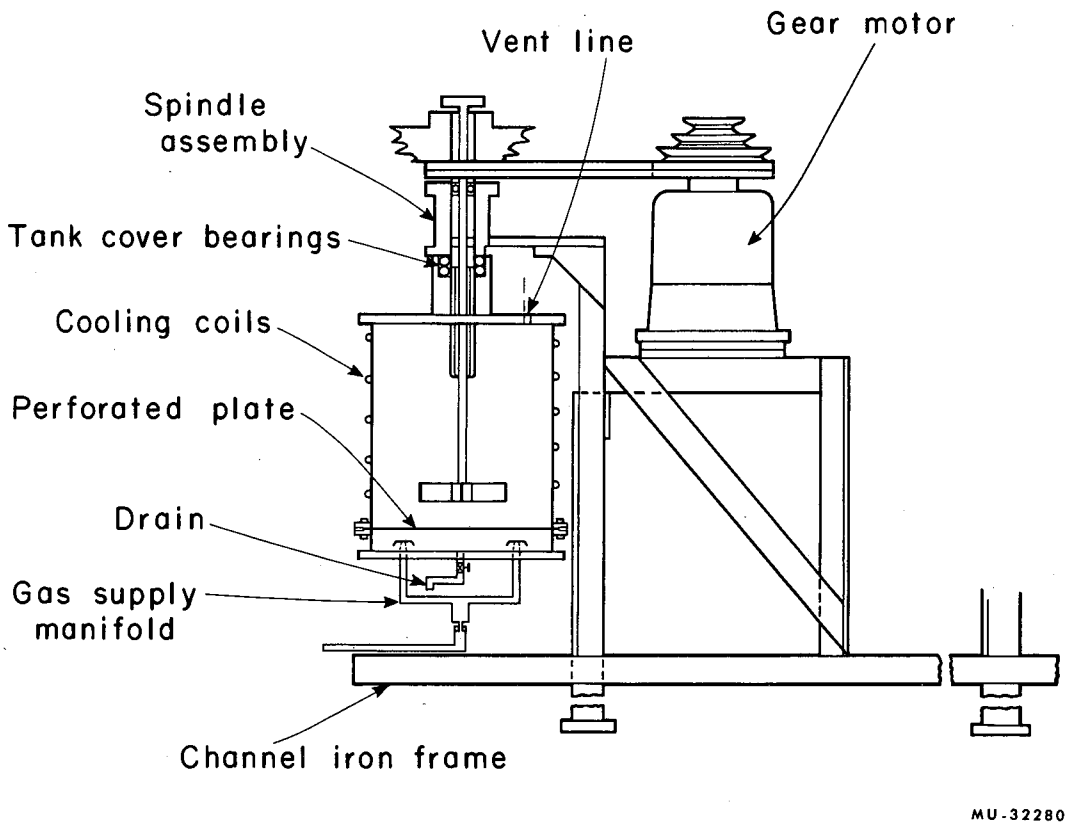

Fig. 1. Mixing vessel, drive assembly, and stand.

Table I. Physical dimensions of experimental equipment.

Impeller dimensions

Impeller number	Length (in.)	Width (in.)	Number of blades
A-1	5.00	1.00	4
A-2	5.00	2.00	4
A-3	6.00	1.625	4
A-4	5.00	3.00	4
A-5	3.00	3.00	4
B-1 (Turbine)	5.00	1.25	4

Tank dimensions

Inner diameter = 10.0 inches

Inside height of liquid section = 16.0 inches

Sampling Probe

The probe used for volumetric sampling of the contents of the tank was a length of stainless steel tubing, of 3/16 in. o. d. and 1/32 in. i. d. The probe ended in a horizontal arm 3 in. long, with the inner diameter tapered out to 1/16 in. and the outer portion tapered to yield a fine-edged wall at the probe end. The probe tube could be rotated and moved vertically through a packing gland which attached to the tank cover. A Lucite handle was attached to the exterior part of the tube; and a protractor mounted on the tank cover allowed determination of the radial probe position within the tank. The array of sampling points adopted is shown in Fig. 2.

In order to facilitate the sampling procedure, a volumetric sampling apparatus was constructed which consisted of a 30-ml calibrated glass pipet fitted with vacuum-joint stopcocks at each end. A Duo-Seal vacuum pump was used to evacuate the pipet; afterward it could be closed and connected to the sampling probe by flexible rubber tubing so as to sample the tank contents.

Analysis of the initial data showed that they varied with the angle between the probe axis and the local direction of flow. In order to determine the orientation giving the most representative gas and liquid proportions, an additional probe was constructed of the same type of tubing with the same entrance design, but with a U-shaped bend to permit sampling at a single radial point in the tank while varying the angle.

Conductivity Probe

A conductivity probe was designed to measure the location of the upper liquid surface. This was connected to a 12-volt battery, in series with a milliammeter (with 1.0 mA full scale) and a resistance box. The probe was constructed of hollow 3/16-in. stainless steel tubing through which the insulated leads were threaded and then sealed 3/16-in. apart into a Lucite end piece. The whole probe was then insulated with epoxy-resin glue. The probe was inserted into the tank through the same packing gland as the sampling probe.

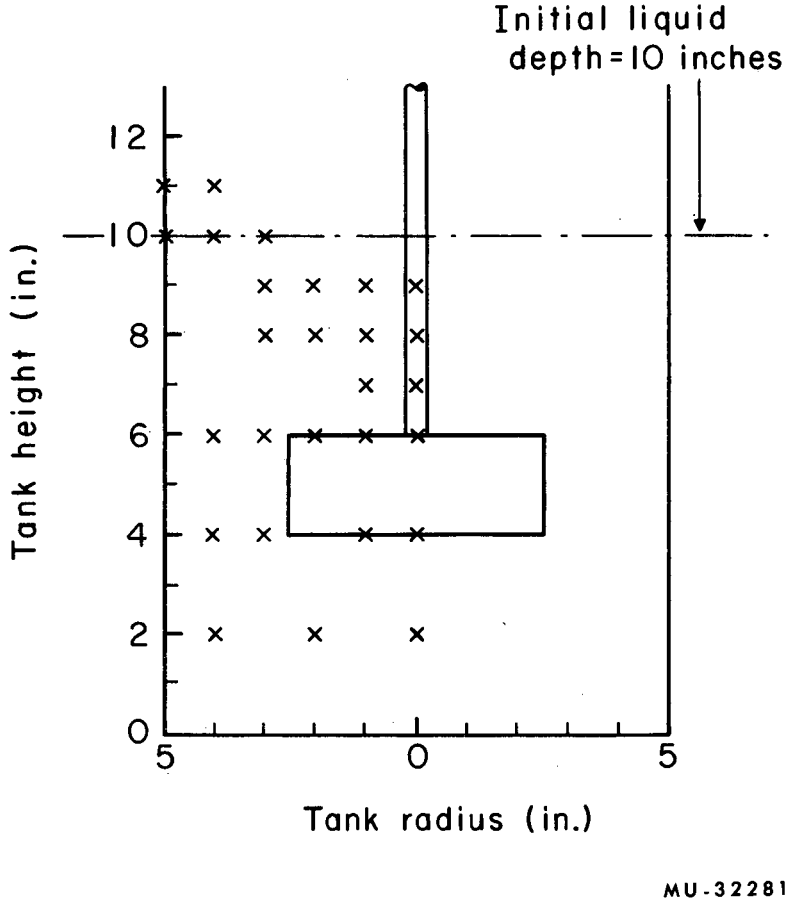

Fig. 2. Array of gas-liquid sampling points in mixing vessel.

When work was done with organic liquids, their low conductivities required a 200-volt source and a variable ammeter capable of reading 1 μA, since the conductivities of the pure liquids were in the range of 0.01 to 0.05 mA.

Gas System

The gas supply system consisted simply of a cylinder of compressed air, a double reducing valve, and a wide-range rotameter. Flexible Tygon tubing was used to the stand below the tank, where a 1/2-in. brass delivery tube connected into the 1/4-in. copper-tubing manifold through an O-ring rubber gasket, thus ensuring free rotation of the tank above. The copper tubing divided into a four-sided manifold which delivered the gas into a hollow chamber below the perforated bottom plate of the mixing vessel (Fig. 1). A cap similar to a distillation-column bubble cap was used to divert the gas flow as it entered the hollow chamber, thus preventing any excessive localized flow through the perforated plate.

Materials

Properties of the liquids studied are given in Table II.

Operating Procedure

For each run, 12.85 liters of liquid (needed to bring the liquid height in the tank to 10.0 inches) was measured out at 20° C. Air flow was started, to prevent drainage of liquid through the air-inlet holes, and the liquid was added to the tank. The temperature of the tank contents was then adjusted to 20° ± 0.5°C by circulating water through the cooling coils.

A nylon monofilament line was used for supporting the weights used for the torque determination. Since the torque reading tended to oscillate at higher speeds, it was necessary to take a mean value between the extremes of the oscillations. At lower speeds the coefficient of static friction was significant, and a mean value of the force was obtained by approaching the position of rest from both sides.

Table II. Physical properties of materials utilized.

Liquid	Density (g/cc)	Surface tension (dynes/cm)	Viscosity (centipoises)
Ethylene glycol (soln.)[a]	1.1015	57.0	13
Isopropyl alcohol	0.785	21.5	2.3
Water	0.008	72.0	1.0
Carbon tetrachloride	1.595	26.8	0.97

[a]Mixture of ethylene glycol (87%) and water. Since ethylene glycol is hygroscopic, specific gravity of the mixture was taken before and after each run to take into account the water absorbed (actually, in the range of 1% or less) during the run.

The impeller speed was determined by using an electric stop watch and the microswitch electronic counter. In order to verify that the impeller speed remained constant for a fixed pulley arrangement, the speed was measured during each run; no significant variation was observed.

In plotting the shape of the upper liquid surface, preliminary mapping of the whole surface with the conductivity probe indicated that placing the probe at the root-mean-square (or mean-area) radius gave a mean height equivalent to the result obtained by integration under the actual liquid surface. Since the surface was in a constant state of agitation, it was necessary to take a conductivity value half that of the continuous liquid phase as representing the actual surface position.

Since the power dissipation reached a constant value within a few seconds, a waiting time of 60 seconds was deemed fully adequate for establishing equilibrium within the system. When the sampling apparatus was used, a check of the power showed no measurable increase due to the insertion of the small-diameter stainless steel tubing. On the average, five samples were taken at each point within the tank; the time of actual fluid flow during the sampling was around 20 seconds. The probe was periodically recalibrated in pure liquid to ensure that the same vacuum was achieved before each sample and that the results were therefore consistent.

INCIPIENT VORTEX FORMATION

Early in the course of the experimental work on gas-liquid mixtures, it became necessary to measure the pure-liquid power input as a reference condition. In order to examine this behavior, the perforated bottom plate was removed and a solid plate inserted. Upon calculation of the values of the power number for the A-2 impeller, it was found that the highest speed resulted in a large reduction in P_0. The phenomenon was then systematically explored with both water and carbon tetrachloride.

Figure 3 illustrates the behavior for various impeller sizes for both carbon tetrachloride and water. As was pointed out earlier, the initial value of P_0 varies owing to the difference in impeller dimensions. The effect of impeller depth is the same for all the runs; i.e., when the impeller is closer to the liquid surface, the decrease in P_0 is more pronounced and begins at a lower speed. This appears to be due to the increase in the upper-surface velocity components as the impeller is brought closer to the top of the liquid.

Figure 4 shows the general correlation of all the experimental data obtained; the Froude number N^2L/g is used as the dimensionless impeller-speed group(here g is gravitational acceleration). In order to verify the choice of the Froude number the runs with carbon tetrachloride were made, providing a change of liquid density from 1.0 to 1.6 g/cm^3, and of surface tension from 72 to 26.8 dynes/cm. The general correlation indicates clearly that Froude number, rather than Weber or Reynolds number, is the proper correlating variable. The Froude number is further justified by dimensional analysis[1] and by experimental observations,[18] for vortex formation in an agitated unbaffled cylindrical vessel. The introduction of the geometrical factor $G_v = L^2W/T^2H$, the impeller-to-tank-volume ratio, brings the break points of the curves for different impellers to the same value, while Z/H accounts for the described effect of impeller depth. Here Z is the distance from the center of the impeller to the tank bottom.

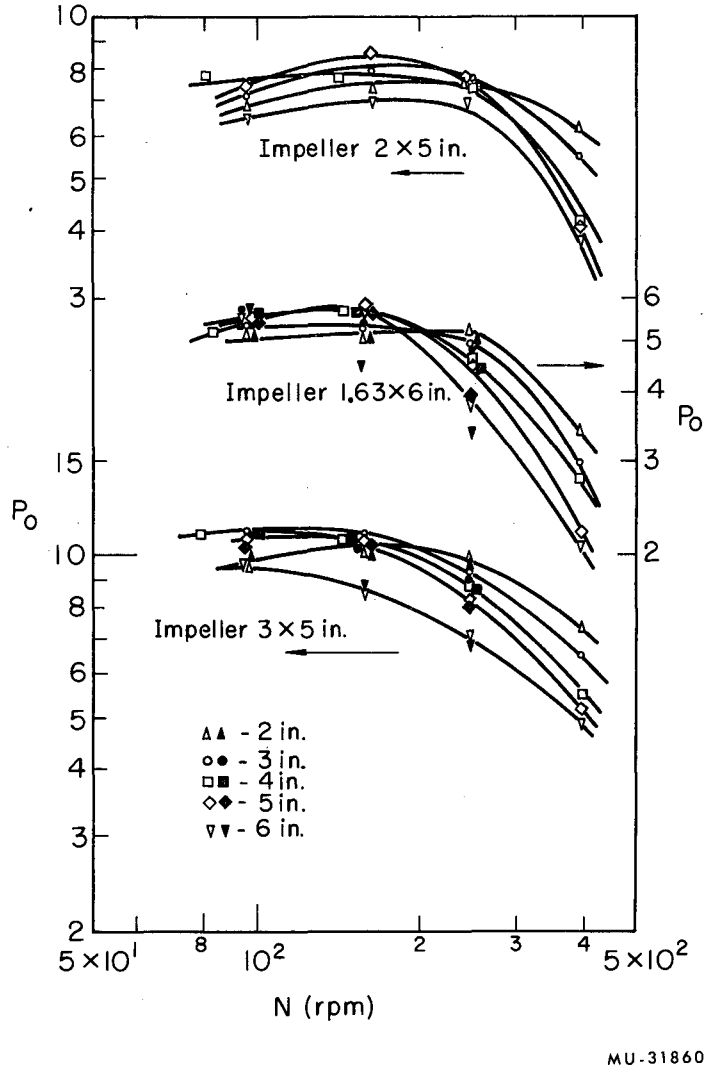

Fig. 3. Effect of speed on power number at different distances between bottom edge of impeller and bottom of vessel.

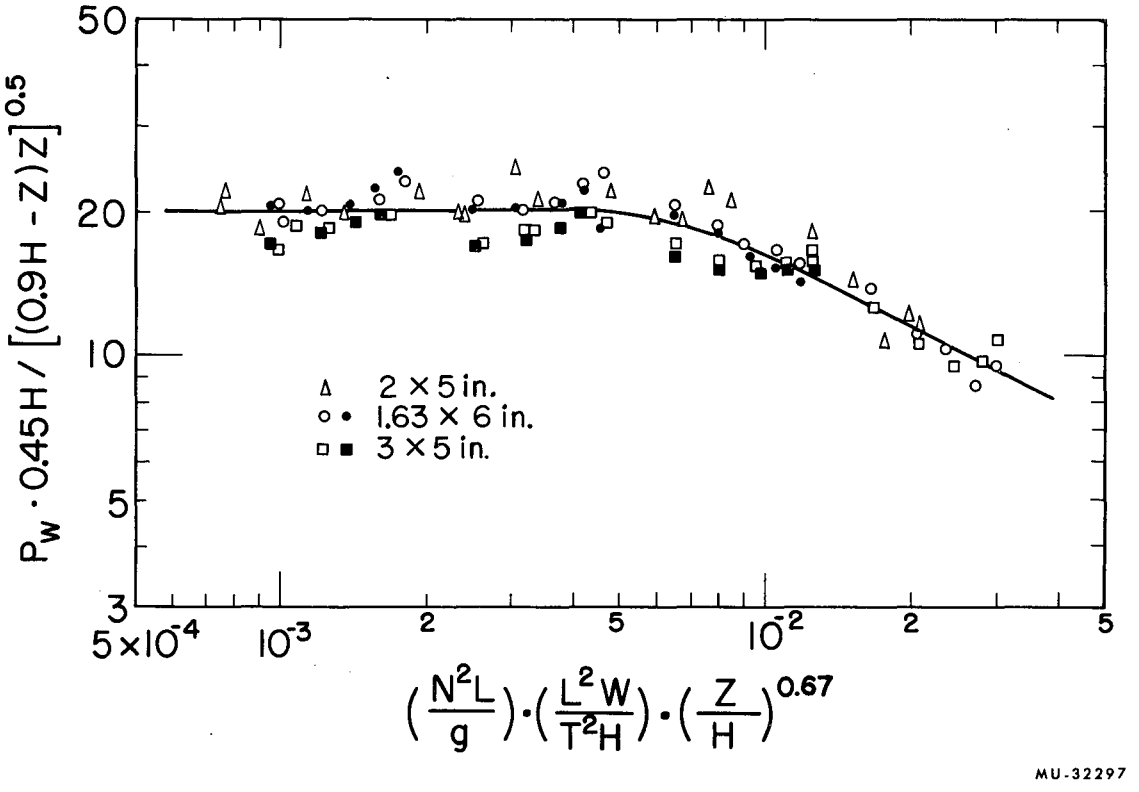

Fig. 4. Correlation of power number for various impeller sizes and positions.

In order to correct the initial power behavior, the modified power number P_w was used, along with an empirical correction factor s for impeller depth given by

$$s = (0.9H/2)/(0.9H-Z)^{1/2}(Z)^{1/2} . \qquad (4)$$

This factor is seen to be nearly symmetrical in Z and $H-Z$, i.e., about the mid-height of the tank. The slight asymmetry is due to a difference in the effects of the lower and upper liquid boundaries. The results of this general correlation are shown in Fig. 4. As can be seen from the curve, a definite critical value of the correlating function occurs at the value of $N_{Fr}(L^2W/T^2H)(Z/H)^{2/3} \approx 5 \times 10^{-3}$. Thus an increase of impeller speed and size or an increase of Z tends to bring about the onset of the vortexing action.

In order to rule out the possibility that the decrease in P_0 is due only to circular motion of the fluid, the experiment was also carried out in a closed tank. Here the characteristic reduction in power number did not occur. The phenomenon can therefore be attributed to introduction of air from the free liquid surface which then mixes down into the impeller region.

To investigate this apparent introduction of air downward into the liquid, an experimental probe was used to determine the density of the tank mixture at various points within the tank. Figure 2 shows the aggregate of sampling points within the tank. Since the actual data were somewhat erratic, and appeared to indicate a dependence on orientation of the sampling tube, a second tube was designed to sample at one point, but with various angular positions. As can be seen from Fig. 5, the 90° orientation (directly into the field of flow) gives the lowest values of ϕ. It appears that, owing to its much lower viscosity, the gas enters the small sampling tube more readily than does the liquid, particularly if the tube is orientated away from the flow field at 180°. In this orientation a wake or low-pressure region would probably form, making the preferential sampling of gas more likely. Figure 6 shows the final plot of volume-percent air for various locations within

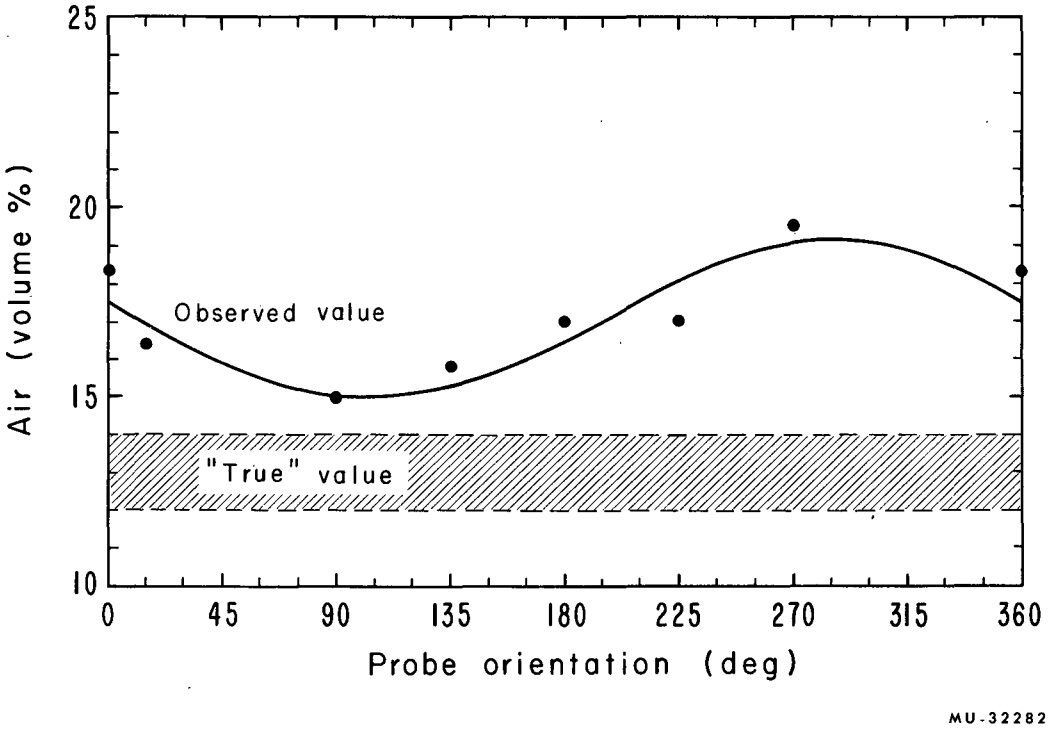

Fig. 5. Effect of probe orientation upon observed volume fraction of gas phase.

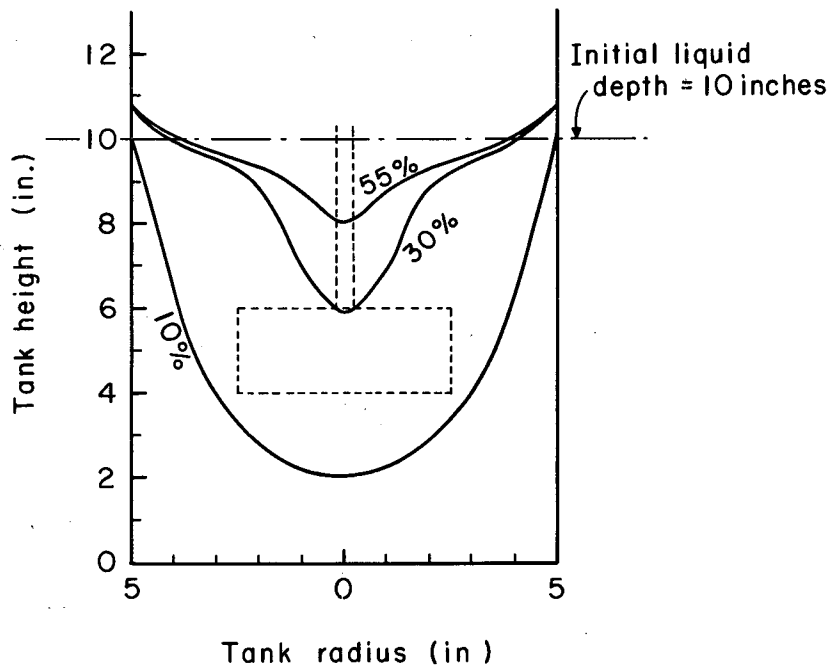

Fig. 6. Contours for volume fraction of air in baffled open-top vessel; impeller A-2, 393 rev/min.

the tank. These values are corrected for probe orientation, but still appear to be slightly high in gas concentration, owing to the previously discussed sampling tendency.

The actual mechanism whereby the gas is introduced into the liquid was next explored. Visual observation, along with a systematic exploration using the sampling apparatus just described, indicated a behavior previously reported by Taylor and Metzner[13,19] (shown in Fig. 7), which they observed with the aid of photographic techniques in a glass-walled vessel.[19] As Taylor and Metzner observed, a "surface" or region of high shear exists where fluids flowing in opposite directions meet. This is caused by the action of the baffles in changing the tangential flow to vertical flow. This "surface" does not remain stationary, but appears to be in random oscillatory motion. It is along the upper ridge or seam made by this surface that air is introduced into the liquid, and subsequently carried downward into the impeller. This gas causes a decrease in P_0 in much the same manner as if it were introduced from below.

The use of the Froude number to correlate surface phenomena of this type is not surprising, since N^2L/g gives the ratio of inertial to gravitational forces. Thus the amount of gas introduced (and therefore the power behavior) is strongly dependent upon the velocity components near the upper liquid surface. The strong functional dependence of the drop-off due to impeller height, pointed out earlier, supports the surface-velocity theory.

In summary we see that "incipient vortex formation" is a surface phenomenon, correlated by the use of the Froude number. As N_{Fr}, Z, or L^2W/T^2H is increased, the upper-surface velocity components are increased, bringing about a reduction in the value of the power number when a certain critical value of the correlating function of these variables has been reached.

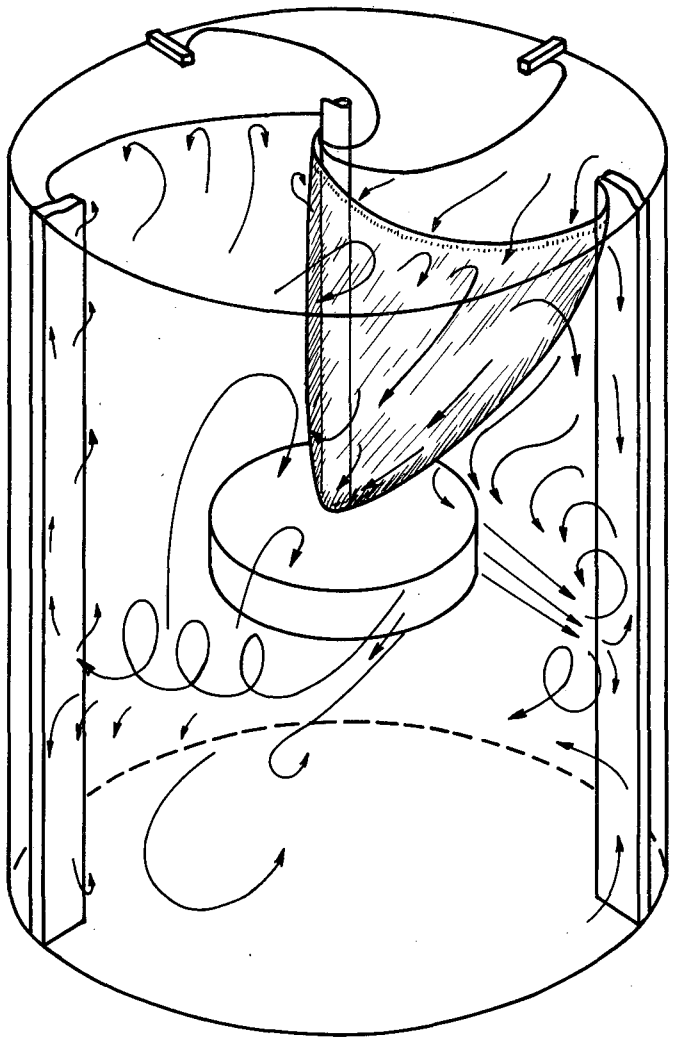

MU-31861

Fig. 7. Flow pattern in baffled open-top vessel at high agitation speed; courtesy J. S. Taylor (reference 13).

POWER REQUIREMENTS FOR GAS-LIQUID MIXTURES

In an agitated liquid system into which a gas is suddenly introduced, there is a sizeable reduction in the power input to the agitator. No suitable explanation for this power reduction is presently available in the literature. Also, existing experimental correlations that utilize dimensionless plots of Q_g/ND^3 versus P/P^* are not in good agreement; therefore a more general correlation of the quantitative behavior of these systems is desirable.

It has been known for some time that the phenomenon of cavitation, whereby a bubble or series of bubbles of liquid vapor forms on an impeller surface, can seriously affect the power characteristics of the impeller. Birkhoff and Zarantonello,[2] in studies of flow perpendicular to a flat disc, find that the presence of a gas in solution reduces the pressure difference necessary for cavity formation. "When the cavity contains air the cavity pressure p_c may differ only slightly from p_f (the fluid pressure), and so the cavity volume is determined more by the amount of this air than by the velocity." In view of this observation it appears quite probable that the presence of a free gaseous phase in the impeller region could greatly reduce the speed necessary for cavity formation (i.e., adhesion of gas to the impeller).

If cavity formation does account for the power reduction, channeling the gas flow into the impeller region would tend to maximize this undesirable effect and should therefore be avoided. The perforated-plate design for a gas sparger appears to provide the best inlet conditions for avoiding channeling of gas flow through the tank. Also, since this method achieves the most homogeneous feed, it should be an excellent experimental reference condition.

The experimental data of this work, which were obtained by utilizing the entrance conditions outlined above, can be found in Tables III through XIV in the Appendix. Figures 8 and 9, and 12 through 14 in the Appendix, show these data superimposed on the published Q_g/ND^3-versus-P/P^* correlation. The curve given by Hyman shown on these plots is an average value, resulting from a survey of the

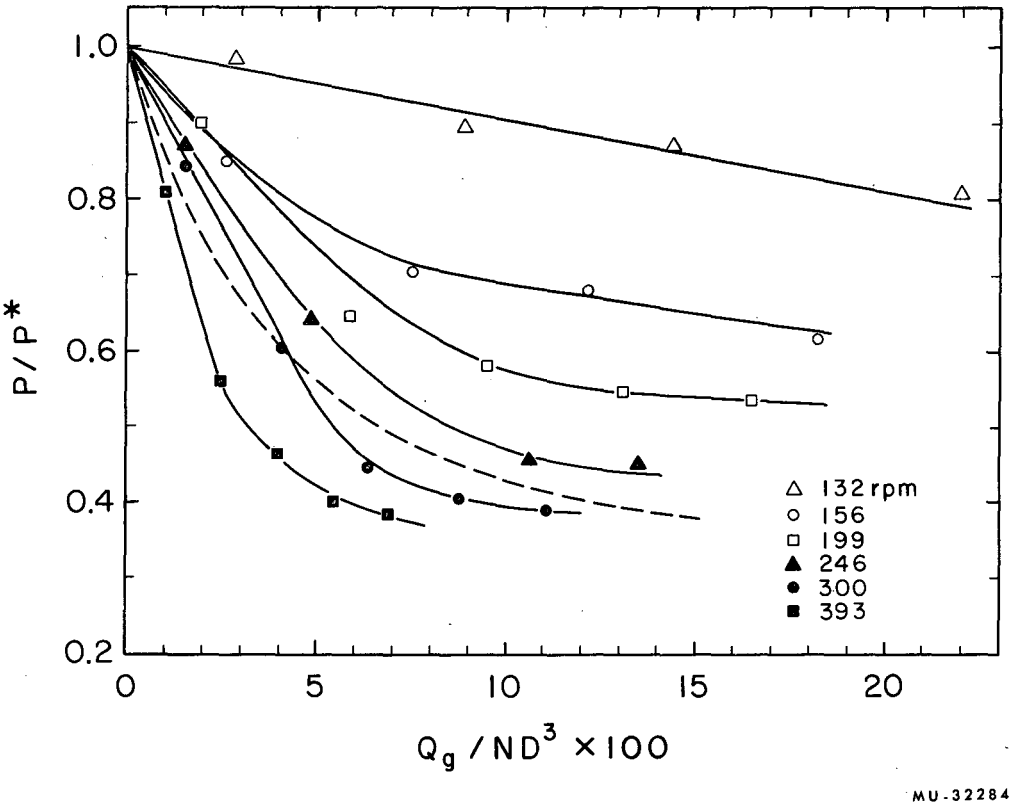

Fig. 8. Ratio of two-phase to single-phase power consumption, as function of ratio of gas flow to impeller flow; impeller A-1. --- Curve given by Hyman.

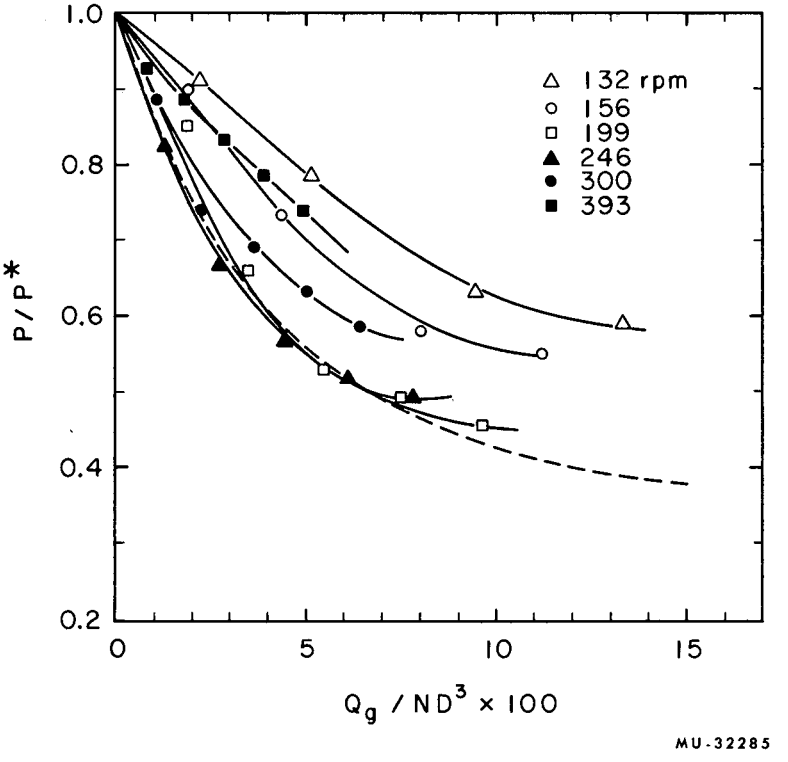

Fig. 9. Ratio of two-phase to single-phase power consumption, as function of ratio of gas flow to impeller flow; impeller A-3. --- Curve given by Hyman.

available experimental data. Figure 8 for the 5 × 1-inch impeller clearly indicates that the effect of impeller speed is not accurately represented by the curve given by Hyman. Figures 9 and 12 through 14 also show the same sort of deviation, with impeller speed, from Hyman's correlation.

It should be noted that impellers A-1, A-5, and B-1 show a continuous downward trend of the curves with impeller speed, whereas A-3 and A-4 give a reduction in P/P* with increasing speed at low speeds, followed by a rise in the P/P* curves at the higher speeds. This can easily be explained by the fact that the reference power, P*, also is in a two-phase system because of incipient vortex formation in the reference liquid. If the value of P* for impellers A-3 and A-4 is corrected to true single-phase behavior by using $P_w = 20$, the continuous downward trend is again assumed. This correction will therefore be used in the ensuing correlation of the experimental data, given in Fig. 10.

It is known that Weber number is the dimensionless function of impeller velocity most often encountered when dealing with two-phase phenomena involving bubble formation. In order to verify a dependence on Weber number in the present system--i.e., to dismiss the possibility of a Froude- or Reynolds-number dependence--several runs were also made with isopropyl alcohol and ethylene glycol. Thus the surface tension was varied from 72 dynes/cm to 21.5 dynes/cm; the viscosity from 1.0 cp to 13 cp; and the density from 1.1 to 0.785 g/cm^3. Since little or no viscosity effect was encountered, and since surface tension was found to have essentially the predicted effect, these runs definitely confirmed the Weber-number dependence of the power behavior.

The geometrical group, $G_v = L^2W/T^2H$, was again found to be the correlating factor for the various impeller sizes. Since this is the ratio of impeller volume to tank volume, it represents the amount of flow achieved at a given impeller speed. As P/P* is

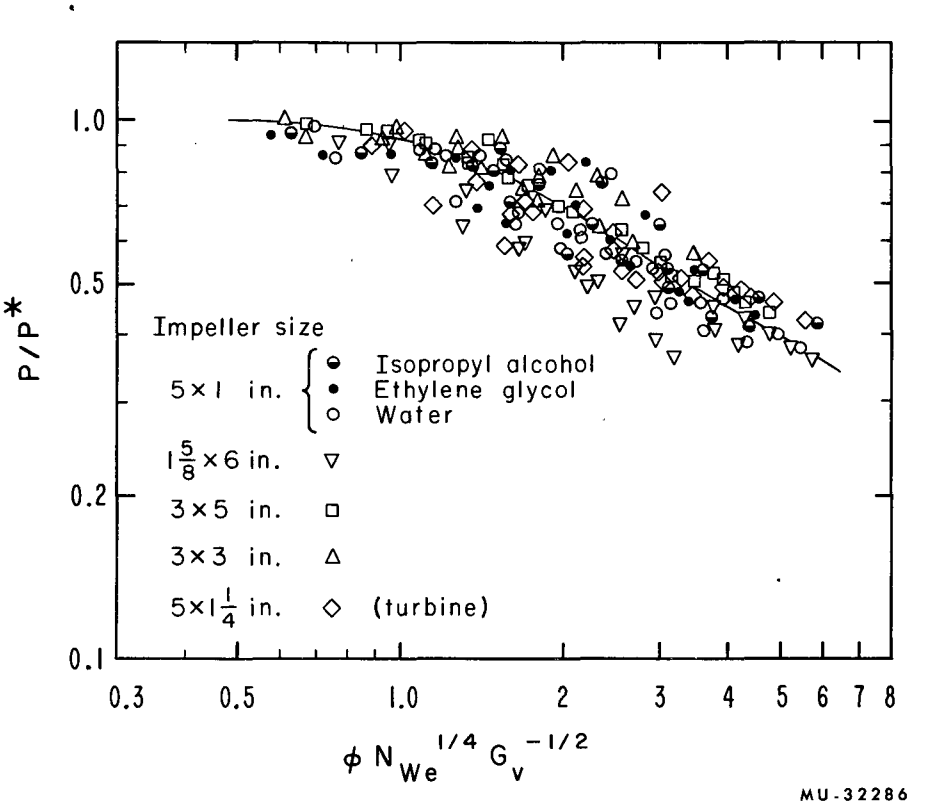

Fig. 10. Correlation of two-phase—to— single-phase power ratio, based on gas holdup, Weber number, and a geometrical factor.

reduced when the flow is reduced, a negative exponent would appear likely for G_v in correlating the power ratio; a value of $G_v^{-1/2}$ was found to bring the various curves together. It is interesting to note that the geometrical factor works equally well for the flat paddle and the turbine data.

GAS HOLDUP

Another important factor is the gas holdup that can be achieved under given agitation conditions. Figure 11 illustrates the holdup behavior for the three liquids used in this work, with the total holdup ϕ equal to $(\phi_0 + \Delta\phi)$. In Fig. 11 the holdup with no agitation, ϕ_0, is plotted against gas flow rate per unit area, $Q_g/(\pi/4)T^2$, for each liquid; and the dimensionless function $\Delta\phi\,(W/H)^{-2/3}\,N_{We}^{-3/4}\,(P/P^*)^{-1/2}$ is plotted against the same abscissa.

These curves furnish a good basis for interpolation or extrapolation of agitation conditions to obtain a fairly accurate estimate of the holdup. Figures 15 through 20 (in the Appendix) illustrate the accuracy of this method; the experimental points are shown with the holdup curves obtained from the general correlations of Fig. 11.

If we assume that the holdup of gas in the impeller region does not vary much from the overall tank holdup, and also that the volume percentage of gas in the impeller region is the major controlling factor in the P/P^* behavior (which definitely appears to be the case), then Figs. 10 and 11 offer a good means of relating P/P^* and ϕ for any gas-liquid system. Thus the ϕ values in the incipient-vortex system can be estimated by using a constant P_w^* for the conditions prior to vortexing, and equating P_w/P_w^* in that system with P/P^* in the holdup correlation.

Another potential application of the relation between P/P^* and ϕ is for a fundamental correlation of Williams's data[21,25] on bubble sizes in agitated gas-liquid mixtures. These studies showed that the mean bubble diameter, d_p, varies inversely with the 1.4 to 1.9 power of impeller speed; this is a greater dependence on speed than in liquid-liquid breakup, (except for the shear breakup observed in a case of high impeller-top speed and high density difference between phases[8]), but less than the dependence suggested by Levich in Eq.(3). Hinze's analysis of the liquid-liquid system[9] shows that the rotational-velocity term in the Weber number comes from the power input (divided by the volume swept out by the impeller). Thus, from a theoretical standpoint, the velocity should be multiplied by the ratio

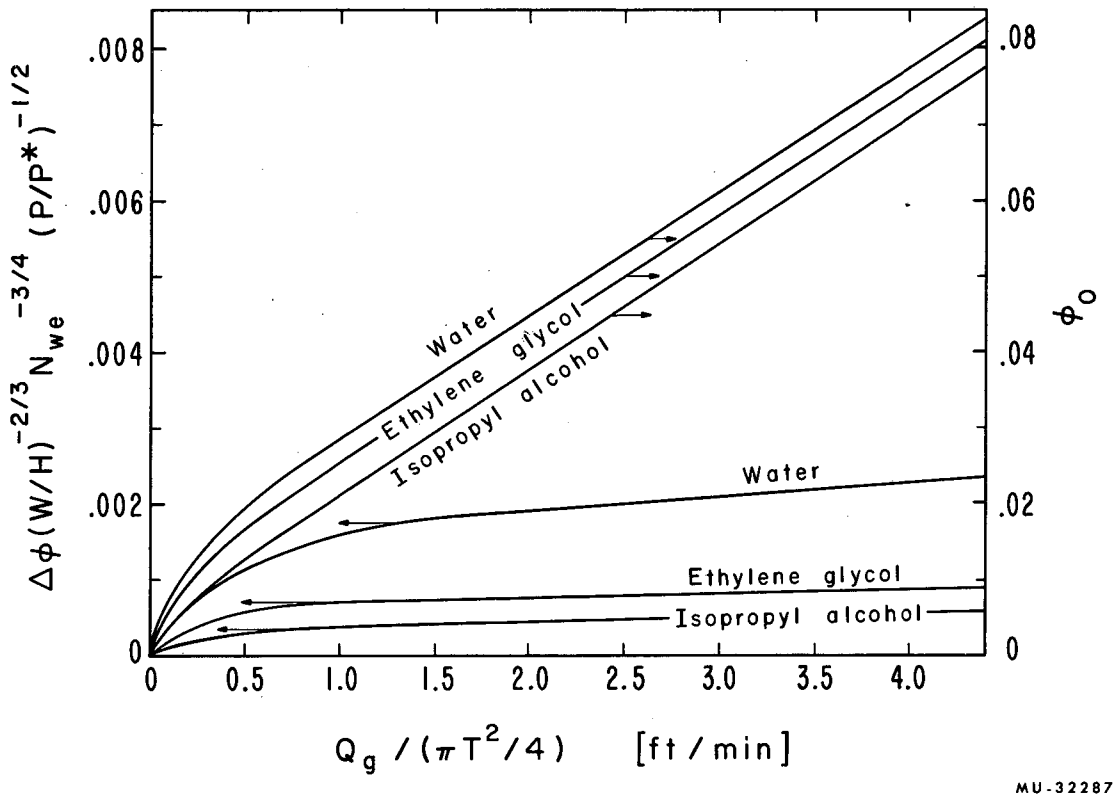

Fig. 11. Correlation of gas holdup based on gas flow, physical properties, and agitation conditions.

$(P/P^*)^{1/3}$ to correct it for cavitation behavior. The problem is further complicated by the probable occurrence of coalescence between the impeller tip and the points where bubble size was measured; Vanderveen[20] has shown for liquid-liquid systems that the combined effect of breakup and coalescence on droplet diameter is given by a relation of the form

$$d/L = d_0/L + (\text{constant})\, N_{We}^{-0.45}\, N_{Re}^{0.25}\, fn(\phi), \qquad (4)$$

where the constant depends on physical properties and geometrical factors, and d_0 is the "impeller-tip" value proportional to $N_{We}^{-0.6}$.

The final goal in gas-liquid contacting is usually to achieve mass transfer between the two phases. Because of lack of a good method of predicting the interfacial area in agitated systems, it has been necessary to treat mass transfer in terms of the $k_{0L}a$ product; however, to accurately design contacting equipment, a reliable method of predicting the effective interfacial area is desirable.

Calderbank[3,4], like Williams, utilized a light-scattering technique to determine values of the interfacial area in gas-liquid mixtures. A subsequent correlation based on theoretical work done by Hinze on turbulent dispersions was given for the mean bubble diameter:

$$d = 4.15 \left[\frac{\sigma^{0.6}}{(P/v)^{0.4}\, \rho_c^{0.2}} \right] \phi^{1/2} + 0.09. \qquad (5)$$

Calderbank explains the holdup term, which is not predicted by theory, by coalescence effects. At higher impeller speeds, much larger values of interfacial area were found to occur, thus the above expression was stated to apply only for $N_{Re}^{0.7}(ND/V_s)^{0.3} < 20{,}000$. This decrease in bubble size below the predicted value was attributed to bubble recirculation and aeration from the free surface. Although a power correlation was given in this work, it was in the unsatisfactory form of Q_g/ND^3 versus P/P^*. Thus it appears that the general correlation for power behavior that we present would be quite useful in combination with an expression of the form of Eq. (5).

The viewpoint on which this study was based, and also the work of Calderbank, is that analysis of the physical factors separately influencing interfacial area and the mass-transfer coefficients in each phase is likely to provide the most general understanding of heterogeneous gas-liquid absorption and reaction processes. A contrary view has been expressed by Westerterp et al.[23], who undertook to determine the effective mean interfacial area by dividing the experimental rate of a reaction (known to be controlled by liquid-phase mass transfer) by the known or predicted mean mass-transfer coefficient. Their results indicated two distinct regions of impeller speed: (a) below a certain speed N_0L there was no effect of impeller speed; and (b) above N_0L the interfacial area was found to vary linearly with speed. Thus a final correlation was presented in the form

$$\frac{aH}{1-\phi} = C(N-N_0)\,L\sqrt{\frac{PT}{\sigma}} \quad ,$$

where a = interfacial area per unit volume, and $C = (0.79 \pm 0.16)\,\mu$ with μ in cp.

The Westerterp approach applies to reactor design only if the mass-transfer coefficient is reasonably constant throughout the reactor, which does not appear likely. Endoh[6] expresses the view that a large part of the total mass transfer occurs in the impeller region, where physical measurement of the interfacial area is impossible. If this is the case, what is needed is the volume integral of $k_{0L}a$, where both k_{0L} and a are known functions of radial and vertical position in the vessel.

CONCLUSIONS

1. The power required for agitation of a two-phase gas-liquid system in a baffled cylindrical vessel with either four-bladed flat impellers or four-bladed turbines may be predicted from one general correlation given in this work. The physical variables involved are the overall gas holdup, fluid density and surface tension, and impeller length, width, and speed.

2. Gas holdup may be estimated through the use of the correlation presented in this work, which consists of first predicting the zero-impeller-speed curve, then utilizing this to predict holdup for any impeller speed.

3. A sudden decrease in power number in a baffled tank as the impeller speed is continuously increased can be attributed to the introduction of air downward into the agitated liquid. The quantitative behavior of this phenomenon can be predicted from the correlation presented in this work involving impeller speed and dimensions, and fluid density.

RECOMMENDATIONS FOR FUTURE WORK

Further work on two-phase power requirements should be concentrated on obtaining an exact explanation of the physical causes of the large power reduction that is associated with the presence of the gaseous phase. The use of glass-walled tanks, with high-speed photography, appears to be a possible method for investigating the existence of cavities on the impeller surfaces, and also the mechanism of bubble breakup in the impeller region. The work presented here should be extended into vessels of different sizes in order to confirm the geometrical factors that were used.

Theoretical work in this field also should be carried out. Experimental work in an area where theoretical solutions already exist, or can be derived, might help to solve the problems associated with the power behavior. One such possible system would be two-phase Couette flow, since there is already a solution of the Navier Stokes equations for this geometry for a one-phase system. This could be done with either one bubble (for which force balances could be written and solved) or for a variety of gas flow rates.

ACKNOWLEDGEMENT

This work was done in the Lawrence Radiation Laboratory under the auspices of the U. S. Atomic Energy Commission.

NOTATION

a	interfacial area per unit volume, cm^{-1} or ft^{-1}
d	mean diameter of bubbles or drops, cm or ft
g	gravitational acceleration, cm/sec^2 or ft/min^2
g_c	conversion factor between force and mass, g cm/gf sec^2 or lb ft/lbf min^2
G_v	geometrical factor, L^2W/T^2H, dimensionless
H	liquid depth, ft
k_L, k_G	mass transfer coefficient, liquid or gas side, cm/sec or ft/min; k_{0L} is the overall coefficient relative to the liquid side
L	impeller diameter, cm or ft
N	impeller speed, revolutions/min
N_0	critical value of impeller speed,[33] revolutions/min
N_{Fr}	Froude number, N^2L/g, dimensionless
N_{Re}	Reynolds number, $NL^2\rho/\mu$, dimensionless
N_{We}	Weber number, $N^2L^3\rho/\sigma$, dimensionless
P	power input to the impeller, gf cm/sec or lbf ft/min
P^*	power input to the impeller (pure-liquid reference condition)
P_0	power number, $Pg_c/N^3L^5\rho$, dimensionless
P_w	power number, $Pg_c/N^3L^4W\rho$, dimensionless
Q_g	volumetric gas flow rate, ft^3/min
s	impeller-depth correction factor, dimensionless
T	tank diameter, cm or ft
U	fluid velocity relative to bubble interface, ft/min
W	impeller width, ft
Z	distance from center of impeller to tank bottom, ft
μ	fluid viscosity, g/cm sec or lb/ft min
ρ	fluid density, g/cm^3 or lb/ft^3
ϕ	gas-phase volume fraction, dimensionless

ϕ_0 volumetric gas-liquid ratio for zero impeller speed

$\Delta\phi$ = $(\phi - \phi_0)$

σ surface tension, g/sec^2 or ft/min^2

APPENDIX (Tables and figures)

Table III. Power number values for impeller A-2 in water at 20° C.

Impeller speed	P_0	P_w	$\frac{P_w(0.45H)}{[(0.9H-Z)Z]^{0.5}}$	N_{Fr}	$(Z/H)^{2/3}$	$N_{Fr}(Z/H)^{2/3}(L^2W/T^2H)$, $(\times 10^{-3})$
96	6.54	16.3	19.6	0.0333	0.789	1.32
96	7.40	18.5	21.4	0.0333	0.712	1.19
82	8.62	21.5	21.9	0.0333	0.630	0.765
96	7.25	18.1	18.3	0.0333	0.544	0.907
96	6.96	17.4	20.2	0.0333	0.447	0.745
156	6.92	17.3	20.8	0.0863	0.789	3.41
156	8.44	21.0	24.3	0.0863	0.712	3.07
146	7.73	19.3	19.6	0.0863	0.630	2.41
156	7.86	19.6	19.8	0.0863	0.544	2.35
156	7.46	18.7	21.6	0.0863	0.447	1.93
246	6.95	17.3	20.8	0.217	0.789	8.53
246	7.68	19.2	22.2	0.217	0.712	7.68
246	7.52	18.8	19.0	0.217	0.630	6.80
246	7.63	19.0	19.3	0.217	0.544	5.87
246	7.56	18.8	21.8	0.217	0.447	4.83
393	3.85	9.6	11.5	0.554	0.789	21.80
393	4.16	10.4	12.1	0.554	0.712	19.70
393	4.23	10.5	10.6	0.554	0.630	17.40
393	5.57	13.9	14.2	0.554	0.544	15.10
393	6.23	15.5	17.9	0.554	0.447	12.40

Table IV. Power number values for impeller A-3 in water at 20° C.

Impeller speed	P_0	P_w	$\frac{P_w(0.45H)}{[(0.9H-Z)Z]^{0.5}}$	N_{Fr}	$(Z/H)^{2/3}$	$N_{Fr}(Z/H)^{2/3}(L^2W/T^2H)$ ($\times 10^{-3}$)
96	5.50	20.3	23.3	0.0399	0.769	1.79
96	5.40	20.0	21.2	0.0399	0.691	1.61
82	5.18	19.2	19.2	0.0281	0.608	1.01
96	5.35	19.8	20.1	0.0399	0.520	1.21
96	5.17	19.1	20.7	0.0399	0.423	0.98
156	5.65	20.9	24.0	0.1035	0.769	4.65
156	5.77	21.3	22.5	0.1035	0.691	4.18
143	5.66	20.9	20.9	0.0899	0.608	3.68
156	5.35	19.8	20.1	0.1035	0.520	3.14
156	5.23	19.4	21.0	0.1035	0.423	2.56
246	3.70	13.6	15.6	0.260	0.769	11.70
246	4.73	15.6	16.5	0.260	0.691	10.75
246	4.63	17.1	17.1	0.260	0.608	9.15
246	4.98	18.4	18.7	0.260	0.520	7.90
246	5.16	19.1	20.7	0.260	0.423	6.45
393	2.23	8.25	9.55	0.260	0.769	29.90
393	2.16	8.00	8.59	0.260	0.691	26.90
393	2.78	10.3	10.3	0.260	0.608	23.70
393	2.99	11.1	11.3	0.260	0.520	20.30
393	3.43	12.7	13.8	0.260	0.423	16.50

Table V. Power number values for impeller A-4 in water at 20°C.

Impeller speed	P_0	P_w	$\frac{P_w(0.45H)}{[(0.9H-Z)Z]^{0.5}}$	N_{Fr}	$(Z/H)^{2/3}$	$N_{Fr}(Z/H)^{2/3}(L^2W/T^2H)$ $(\times 10^{-3})$
96	10.7	17.8	19.9	0.0333	0.671	1.68
80	10.9	18.2	18.7	0.0242	0.587	1.07
96	11.0	18.3	18.3	0.0333	0.496	1.24
96	9.7	16.2	16.7	0.0333	0.398	0.99
156	8.4	14.0	18.8	0.0863	0.750	4.86
156	10.6	17.7	19.8	0.0863	0.671	4.35
143	10.7	17.8	18.3	0.0725	0.587	3.19
156	10.8	18.0	18.0	0.0863	0.496	3.21
156	10.1	16.7	17.0	0.0863	0.398	2.58
246	7.0	11.7	15.7	0.217	0.750	12.2
246	8.3	13.9	15.5	0.217	0.671	10.9
246	8.8	14.7	15.1	0.217	0.587	9.55
246	9.35	15.6	15.6	0.217	0.496	8.08
246	9.95	16.6	17.0	0.217	0.398	6.50
393	4.83	8.05	10.8	0.554	0.750	31.2
393	5.20	8.65	9.7	0.554	0.671	27.9
393	5.50	9.20	9.5	0.554	0.587	24.4
393	6.45	10.7	10.7	0.554	0.496	20.6
393	7.35	10.6	12.5	0.554	0.398	16.5

Table VI. Power number values for impeller A-3 in carbon tetrachloride at 20° C.

Impeller speed	P_0	P_w	$\frac{P_w(0.45H)}{[(0.9H-Z)Z]^{0.5}}$	N_{Fr}	$(Z/H)^{2/3}$	$N_{Fr}(Z/H)^{2/3}(L^2H/T^2W)$ $(\times 10^{-3})$
95	5.10	18.8	20.4	0.0389	0.423	0.966
95	5.35	19.7	20.0	0.0389	0.520	1.19
95	5.68	20.9	20.9	0.0389	0.608	1.39
95	5.78	21.3	22.5	0.0389	0.691	1.57
95	5.68	20.9	24.1	0.0389	0.769	1.75
155	5.05	18.6	20.2	0.1035	0.423	2.56
155	5.37	19.8	20.1	0.1035	0.520	3.15
155	5.58	20.6	20.6	0.1035	0.608	3.68
155	5.67	20.9	22.1	0.1035	0.691	4.18
155	4.40	16.3	18.8	0.1035	0.796	6.65
246	4.93	18.2	19.7	0.261	0.423	6.48
246	4.73	18.2	19.7	0.261	0.520	7.95
246	4.36	16.1	16.1	0.261	0.608	9.30
246	3.90	14.4	15.2	0.261	0.691	10.6
246	3.36	12.4	14.3	0.261	0.769	11.7

Table VII. Power number values for impeller A-4 in carbon tetrachloride at 20°C.

Impeller speed (rev/min)	P_0	P_w	$\frac{P_w(0.45H)}{[(0.9H-Z)Z]^{0.5}}$	N_{Fr}	$(Z/H)^{2/3}$	$N_{Fr}(Z/H)^{2/3}(L^2W/T^2H)$ $(\times 10^{-3})$
95	9.95	16.6	17.1	0.0324	0.398	0.967
95	10.82	18.0	18.0	0.0324	0.496	1.21
95	11.05	18.4	18.9	0.0324	0.587	1.43
95	10.60	17.7	19.8	0.0324	0.671	1.63
155	10.00	16.7	17.2	0.0862	0.398	2.57
155	10.48	17.5	17.5	0.0862	0.496	3.21
155	10.70	17.9	18.4	0.0862	0.587	3.79
155	10.49	17.5	19.5	0.0862	0.671	4.33
155	8.75	14.6	19.6	0.0862	0.750	4.85
246	9.34	15.6	16.0	0.217	0.398	6.48
246	9.00	15.0	15.0	0.217	0.496	8.08
246	8.70	14.5	14.9	0.217	0.587	9.58
246	8.10	13.5	15.1	0.217	0.671	10.90
246	6.80	11.3	15.1	0.217	0.750	12.20

Table VIII. Experimental data and power-ratio values for air in water using impeller A-1 (20° C).

Impeller speed (rev/min)	P	P/P*	Q_g	$(N_{We})^{1/4}$	Φ	$\Phi(N_{We})^{1/4}\left[\frac{L^2W}{T^2H}\right]^{-1/2}$
132	52.0	.985	0.34	3.42	0.032	0.690
132	47.3	.895	0.84	3.42	0.054	1.165
132	46.0	.870	1.36	3.42	0.066	1.410
132	42.3	.805	2.09	3.42	0.085	1.830
156	72.2	.850	0.36	3.73	0.032	0.755
156	64.3	.708	0.84	3.73	0.054	1.270
156	61.5	.678	1.36	3.73	0.070	1.640
156	55.7	.613	2.05	3.73	0.091	2.140
199	179	.900	0.34	4.22	0.041	1.100
199	128	.643	0.84	4.22	0.059	1.580
199	115	.578	1.36	4.22	0.075	2.000
199	109	.547	1.87	4.22	0.102	2.700
199	107	.537	2.36	4.22	0.111	2.950
246	324	.870	0.34	4.70	0.042	1.220
246	238	.642	0.84	4.70	0.066	1.940
246	173	.468	1.36	4.70	0.081	2.400
246	169	.455	1.87	4.70	0.106	3.130
246	167	.450	2.36	4.70	0.121	3.600
300	550	.845	0.34	5.18	0.048	1.560
300	398	.607	0.84	5.18	0.066	2.150
300	289	.442	1.36	5.18	0.091	2.980
300	266	.407	1.87	5.18	0.111	3.640
300	255	.390	2.37	5.18	0.131	4.280
393	1150	.810	0.34	5.94	0.066	2.460
393	800	.563	0.87	5.94	0.081	3.040
393	663	.467	1.36	5.94	0.106	3.950
393	570	.402	1.90	5.94	0.131	4.900
393	540	.380	2.40	5.94	0.144	5.400

Table IX. Experimental data and power-ratio values for air in water using impeller A-3 (20° C).

Impeller speed	P	P/P*	Q_g	$(N_{We})^{1/4}$	ϕ	$\phi(N_{We})^{1/4}\left[\frac{L^2W}{T^2H}\right]^{-1/2}$
132	198	.908	0.34	3.91	0.0476	0.770
132	172	.788	0.87	3.91	0.0592	0.957
132	139	.638	1.56	3.91	0.0810	1.310
132	129	.592	2.00	3.91	0.1060	1.710
156	313	.897	0.34	4.25	0.0540	0.950
156	257	.736	0.87	4.25	0.0750	1.320
156	203	.582	1.56	4.25	0.0960	1.680
156	193	.553	2.00	4.25	0.1210	2.120
199	600	.850	0.34	4.78	0.0698	1.380
199	464	.657	0.87	4.78	0.0810	1.600
199	376	.532	1.36	4.78	0.1060	2.100
199	349	.494	1.87	4.78	0.1165	2.310
199	324	.458	2.40	4.78	0.1350	2.670
246	930	.690	0.34	5.33	0.0850	1.870
246	743	.489	0.84	5.33	0.1010	2.230
246	637	.419	1.37	5.33	0.1165	2.570
246	586	.387	1.87	5.33	0.1360	2.970
246	553	.368	2.40	5.33	0.1440	3.180
300	1400	.564	0.34	5.87	0.1010	2.450
300	1172	.473	0.84	5.87	0.1210	2.940
300	1090	.440	1.36	5.87	0.1310	3.190
300	1009	.406	1.87	5.87	0.1550	3.760
300	945	.381	2.40	5.87	0.1720	4.170
393	2490	.450	0.34	6.74	0.1350	3.760
393	2380	.428	0.84	6.74	0.1550	4.320
393	2250	.403	1.36	6.74	0.1720	4.780
393	2110	.379	1.87	6.74	0.1880	5.230
393	2000	.360	2.40	6.74	0.2020	5.700

Table X. Experimental data and power-ratio values for air in water using impeller A-4 (20° C).

Impeller speed	P	P/P*	$(N_{We})^{1/4}$	ϕ	Q_g	$\phi(N_{We})^{1/4}\left[\frac{LW}{T^2H}\right]^{-1/2}$
132	163	0.990	3.42	0.0540	0.36	0.674
132	158	0.970	3.42	0.0689	0.84	0.872
132	149	0.903	3.42	0.0910	1.56	1.13
132	144	0.872	3.42	0.1060	2.00	1.32
156	247	0.952	3.74	0.0698	0.36	0.952
156	238	0.915	3.74	0.0810	0.84	1.10
156	219	0.843	3.74	0.0960	1.56	1.31
156	207	0.795	3.74	0.1165	2.00	1.59
199	478	0.925	4.22	0.0960	0.36	1.48
199	427	0.825	4.22	0.1010	0.84	1.55
199	395	0.764	4.22	0.1110	1.36	1.70
199	359	0.698	4.22	0.1260	1.87	1.94
199	350	0.678	4.22	0.1392	2.40	2.14
300	1158	0.633	5.18	0.1350	0.36	2.55
300	1080	0.588	5.18	0.1480	0.84	2.80
300	992	0.548	5.18	0.1600	1.36	3.02
300	955	0.518	5.18	0.1670	1.87	3.16
300	923	0.500	5.18	0.1840	2.40	3.48
393	2180	0.527	5.94	0.1750	0.36	3.79
393	2100	0.517	5.94	0.1840	0.84	3.99
393	2000	0.483	5.94	0.1880	1.36	4.07
393	1920	0.463	5.94	0.1970	1.90	4.28
393	1830	0.442	5.94	0.2190	2.40	4.75

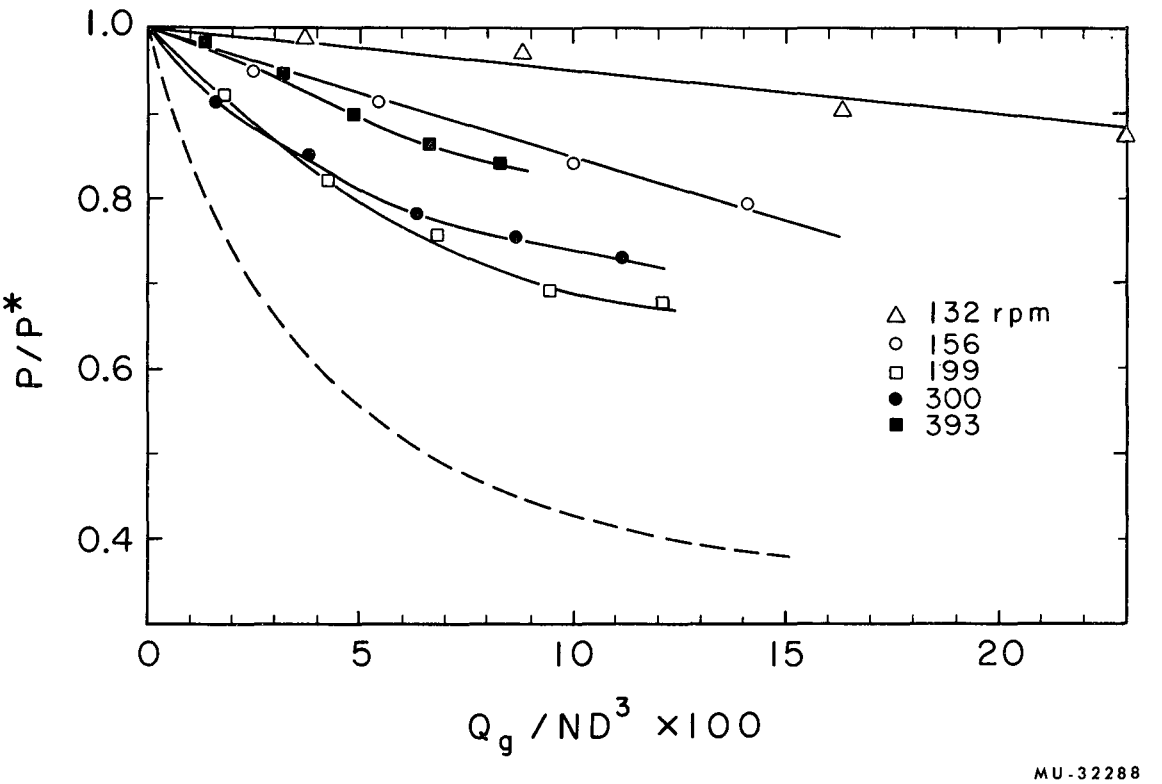

Fig. 12. Ratio of two-phase to single-phase power consumption, as function of ratio of gas flow to impeller flow; impeller A-4. --- Curve given by Hyman.

Table XI. Experimental data and power-ratio values for air in water using impeller A-5 (20° C).

Impeller speed	P*	P/P*	Q_g	$(N_{We})^{1/4}$	ϕ	$\phi(N_{We})^{1/4}\left[\frac{L^2W}{T^2H}\right]^{1/2}$
199	63.5	1.00	0.36	2.80	0.0357	0.607
199	63.5	0.915	0.84	2.80	0.0540	0.920
199	63.5	0.915	1.36	2.80	0.0750	1.27
199	63.5	0.915	1.87	2.80	0.0901	1.53
199	63.5	0.860	2.40	2.80	0.1110	1.89
246	121	0.930	0.36	3.10	0.0357	0.673
246	121	0.870	0.84	3.10	0.0592	1.11
246	121	0.813	1.36	3.10	0.0750	1.41
246	121	0.797	1.87	3.10	0.0960	1.81
246	121	0.797	2.40	3.10	0.1210	2.28
300	206	0.921	0.36	3.43	0.0476	0.990
300	206	0.827	0.84	3.43	0.0592	1.23
300	206	0.745	1.36	3.43	0.0810	1.69
300	206	0.722	1.87	3.43	0.1010	2.10
300	206	0.708	2.40	3.43	0.1210	2.52
393	464	0.883	0.36	3.93	0.0540	1.29
393	464	0.713	0.84	3.93	0.0750	1.79
393	464	0.636	1.36	3.93	0.0960	2.29
393	464	0.597	1.87	3.93	0.1110	2.65
393	464	0.567	2.40	3.93	0.1310	3.47

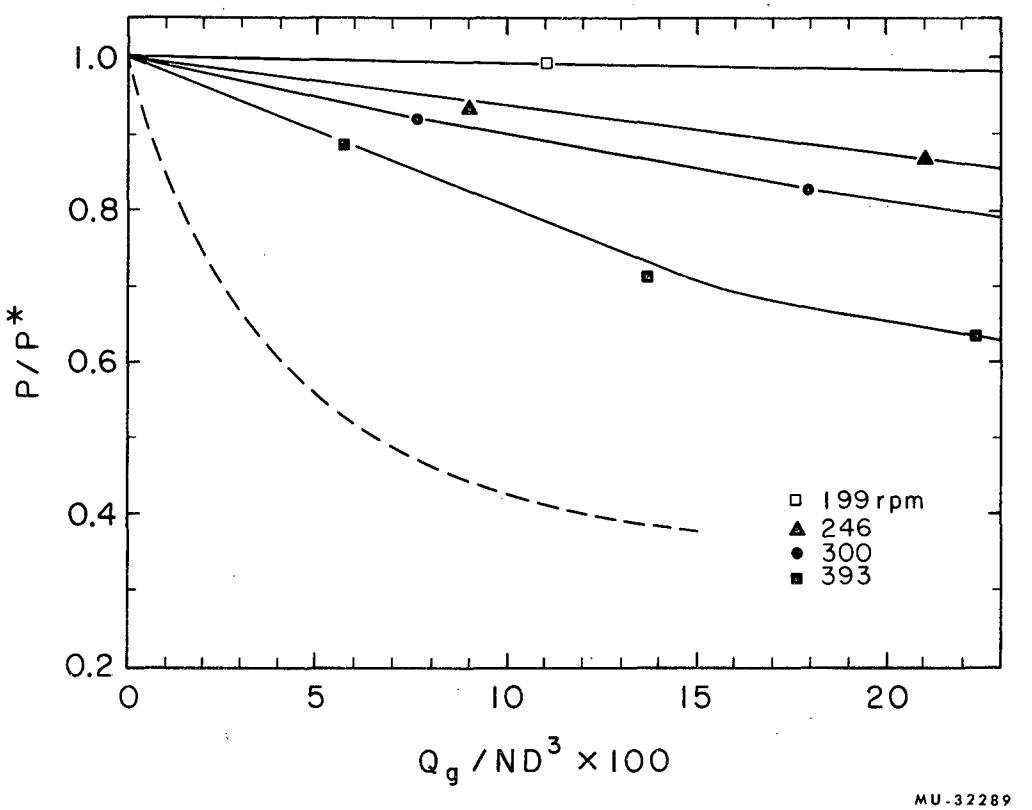

Fig. 13. Ratio of two-phase to single-phase power consumption, as function of ratio of gas flow to impeller flow; impeller A-5. --- Curve given by Hyman.

Table XII. Experimental data for power-ratio values for air in water with impeller B-1 (20° C).

Impeller speed	P*	P/P*	Q_g	$(N_{We})^{1/4}$	ϕ	$\phi(N_{We})^{1/4}\left[\frac{L^2W}{T^2H}\right]^{-1/2}$
132	60.4	0.90	0.36	3.42	0.0413	0.795
132	60.4	0.695	0.84	3.42	0.0593	1.14
132	60.4	0.675	1.36	3.42	0.0810	1.57
132	60.4	0.675	1.87	3.42	0.0910	1.75
156	99.3	0.95	0.31	3.73	0.0476	1.01
156	99.3	0.77	0.84	3.73	0.0655	1.38
156	99.3	0.71	1.36	3.73	0.0810	1.70
156	99.3	0.69	1.87	3.73	0.1010	2.13
156	99.3	0.62	2.40	3.73	0.1165	2.46
199	218	0.87	0.36	4.22	0.0540	1.33
199	218	0.58	0.84	4.22	0.0655	1.56
199	218	0.55	1.36	4.22	0.0910	2.17
199	218	0.54	1.87	4.22	0.1110	2.64
199	218	0.53	2.39	4.22	0.1260	3.00
246	419	0.84	0.36	4.70	0.0592	1.57
246	419	0.54	0.84	4.70	0.0810	2.15
246	419	0.51	1.36	4.70	0.1010	2.68
246	419	0.49	1.87	4.70	0.1165	3.09
246	419	0.46	2.40	4.70	0.1350	3.58
300	720	0.84	0.36	5.18	0.0698	2.04
300	720	0.57	0.84	5.18	0.0850	2.50
300	720	0.52	1.36	5.18	0.1110	3.25
300	720	0.50	1.87	5.18	0.1350	3.96
300	720	0.47	2.40	5.18	0.1480	4.34
396	1910	0.74	0.36	5.94	0.0910	3.03
396	1910	0.55	0.84	5.94	0.1110	3.72
396	1910	0.505	1.36	5.94	0.1260	4.22
396	1910	0.46	1.87	5.94	0.1480	4.95
396	1910	0.43	2.40	5.94	0.1670	5.60

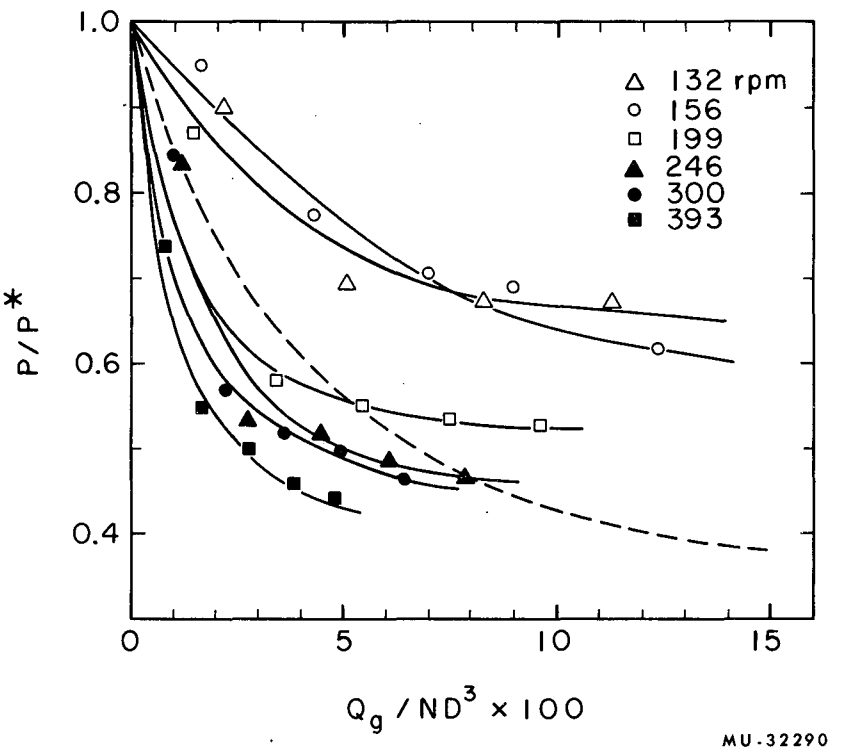

Fig. 14. Ratio of two-phase to single-phase power consumption, as function of ratio of gas flow to impeller flow; impeller B-1. --- Curve given by Hyman.

Table XIII. Experimental data and power-ratio values for air in ethylene glycol using impeller A-1 (20° C).

Impeller speed	P*	P/P*	Q_g	ϕ	$(N_{We})^{1/4}$	$\phi(N_{We})^{1/4}\left[\frac{L^2W}{T^2H}\right]^{-1/2}$
132	55.5	0.935	0.36	0.0250	3.72	0.588
132	55.5	0.870	0.84	0.0413	3.72	0.975
132	55.5	0.850	1.36	0.0540	3.72	1.270
132	55.5	0.827	1.87	0.0655	3.72	1.540
132	55.5	0.827	2.40	0.0810	3.72	1.90
199	195	0.860	0.36	0.0250	4.58	0.725
199	195	0.690	0.84	0.0475	4.58	1.38
199	195	0.645	1.36	0.0540	4.58	1.56
199	195	0.617	1.87	0.0698	4.58	2.02
199	195	0.607	2.40	0.0850	4.58	2.47
300	670	0.763	0.36	0.0413	5.62	1.46
300	670	0.700	0.84	0.0593	5.62	2.10
300	670	0.538	1.36	0.0750	5.62	2.66
300	670	0.482	1.87	0.0910	5.62	3.23
300	670	0.462	2.40	0.0960	5.62	3.40
396	1540	0.840	0.36	0.0540	6.45	2.20
396	1540	0.670	0.84	0.0698	6.45	2.85
396	1540	0.530	1.36	0.0850	6.45	3.47
396	1540	0.477	1.87	0.1010	6.45	4.13
396	1540	0.440	2.40	0.1110	6.45	4.53

Table XIV. Experimental data and power-ratio values for air in isopropyl alcohol using impeller A-1 (20°C).

Impeller speed	P*	P/P*	Q_g	ϕ	$(N_{We})^{1/4}$	$\phi(N_{We})^{1/4}(G_v)^{-1/2}$
132	44.7	0.945	0.36	0.0230	4.37	0.634
132	44.7	0.838	0.84	0.0413	4.37	1.140
132	44.7	0.812	1.36	0.0540	4.37	1.485
132	44.7	0.784	1.87	0.0655	4.37	1.80
132	44.7	0.784	2.40	0.0850	4.37	2.35
199	155	0.870	0.36	0.0250	5.37	0.850
199	155	0.707	0.84	0.0475	5.37	1.610
199	155	0.577	1.36	0.0593	5.37	2.01
199	155	0.564	1.87	0.0750	5.37	2.54
199	155	0.542	2.40	0.0910	5.37	3.08
300	520	0.847	0.36	0.0320	6.58	1.33
300	520	0.645	0.84	0.0540	6.58	2.25
300	520	0.493	1.36	0.0750	6.58	3.11
300	520	0.434	1.87	0.0910	6.58	3.77
300	520	0.418	2.40	0.1055	6.58	4.38
398	1080	0.880	0.36	0.0320	7.60	1.53
398	1080	0.650	0.84	0.0655	7.60	3.13
398	1080	0.530	1.36	0.0750	7.60	3.58
398	1080	0.473	1.87	0.0960	7.60	4.60
398	1080	0.425	2.40	0.1210	7.60	5.90

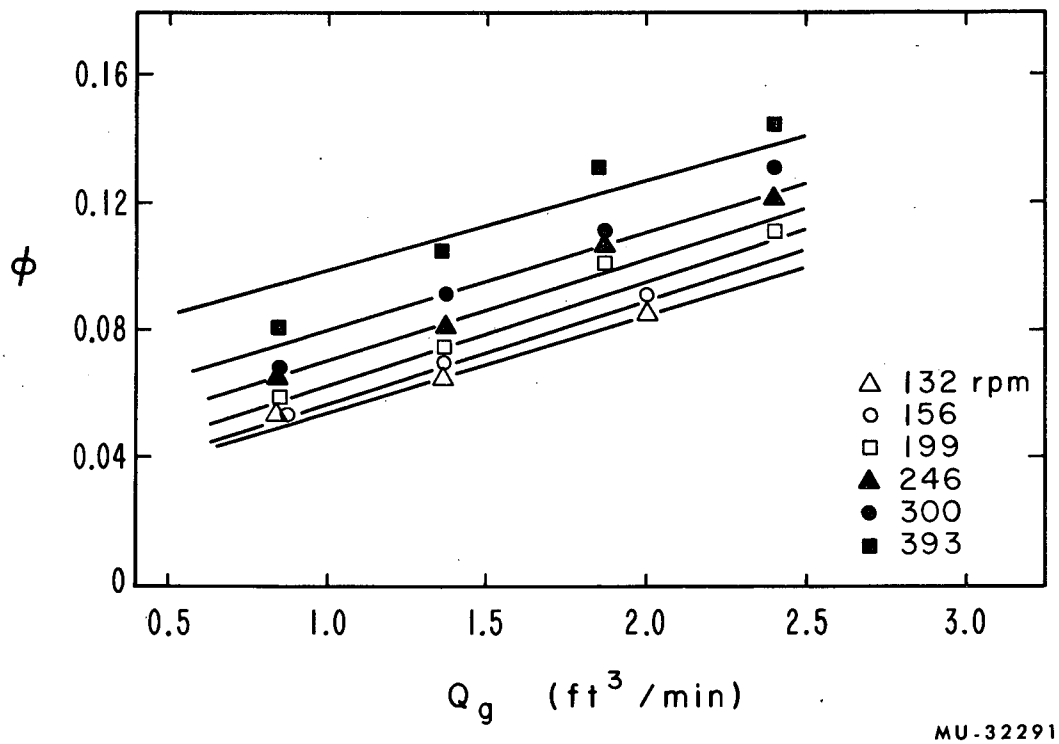

Fig. 15. Gas holdup vs superficial gas velocity; impeller A-1. Points from experimental data; curves calculated from correlation.

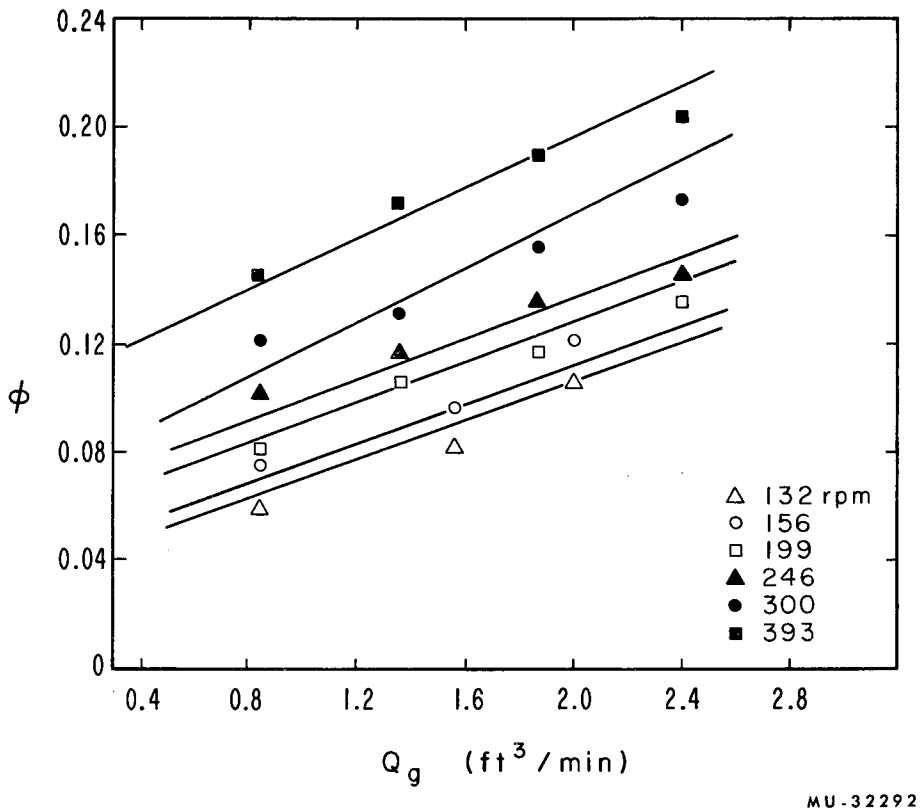

Fig. 16. Gas holdup vs superficial gas velocity; impeller A-3. Points from experimental data; curves calculated from correlation.

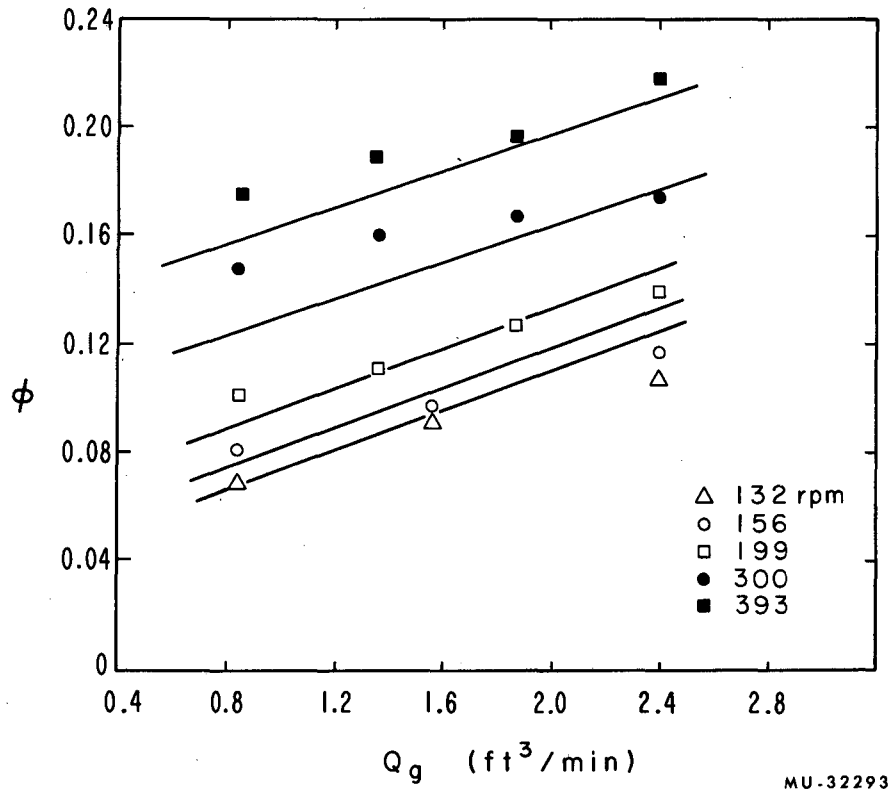

Fig. 17. Gas holdup vs superficial gas velocity; impeller A-4. Points from experimental data; curves calculated from correlation.

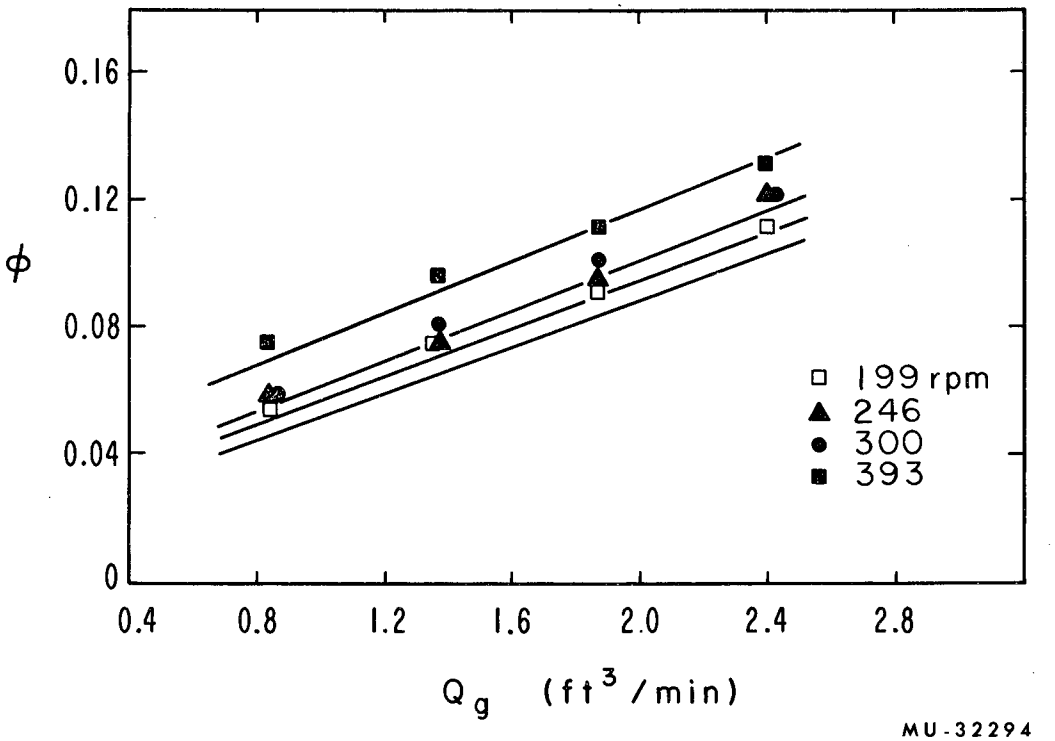

Fig. 18. Gas holdup vs superficial gas velocity; impeller A-5. Points from experimental data; curves calculated from correlation.

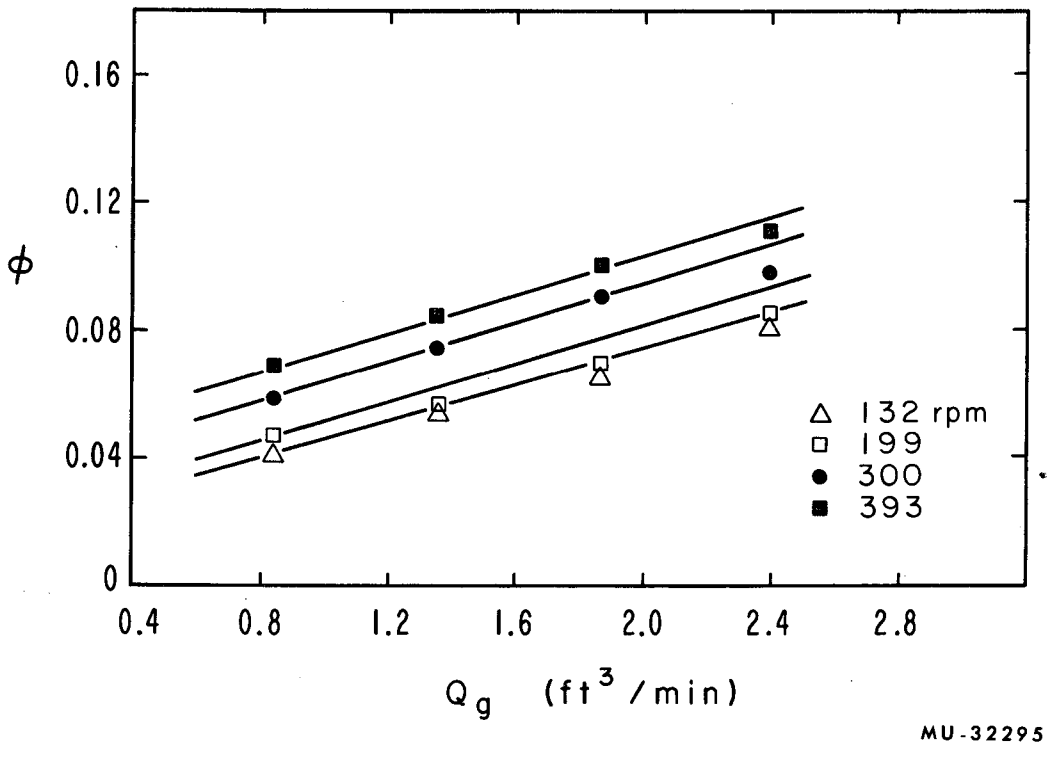

Fig. 19. Gas holdup vs superficial gas velocity; impeller A-1; ethylene glycol–water mixture.

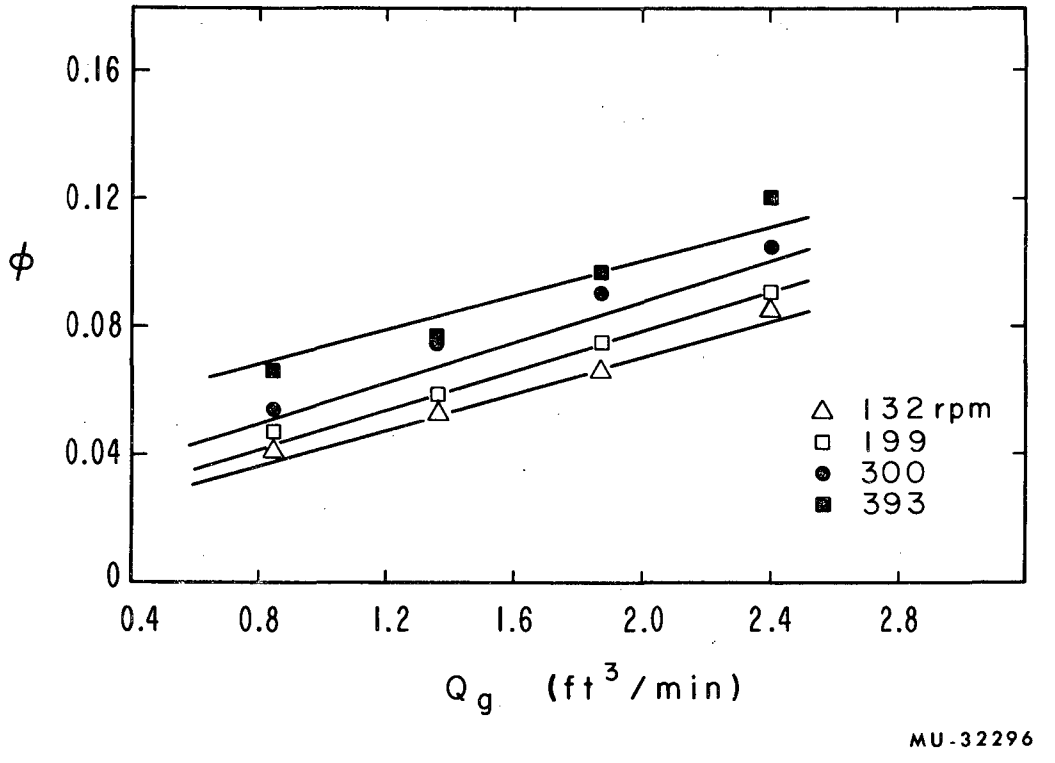

Fig. 20. Gas holdup vs superficial gas velocity; impeller A-1; isopropyl alcohol.

BIBLIOGRAPHY

1. R. B. Bird, W. E. Stewart, and E. N. Lightfoot, Transport Phenomena (John Wiley and Sons, Inc., New York, 1960), p. 108.
2. Garrett Birkhoff and E. H. Zarantonello, Jets, Wakes, and Cavities (Academic Press, Inc., New York, 1957.
3. P. H. Calderbank, Brit. Chem. Eng., 1, No. 8, 209; No. 9, 267 (1956).
4. P. H. Calderbank, Trans. Instn. Chem. Engr., 36, 443 (1958).
5. C. M. Cooper, G. A. Fernstrom, and S. A. Miller, Ind. Eng. Chem. 36, 504 (1944).
6. K. Endoh, Sci. Papers Inst. Phys. Chem. Res. 53, 216 (1959).
7. J. L. Fick, H. E. Rea, and T. Vermeulen, The Effects of Agitator Geometry in the Mixing of Liquid-Liquid Systems, University of California Radiation Laboratory Report UCRL-2545, April 1954.
8. P. L. Fondy and R. L. Bates, A. I. Ch. E. J. 9, 338 (1963).
9. J. O. Hinze, A. I. Ch. E. J. 1, 289 (1955).
10. Daniel Hyman, in Advances in Chemical Engineering, Vol. 3 (Academic Press, New York, 1962), 119-202.
11. G. E. Langlois, J. E. Gullberg, and T. Vermeulen, Rev. Sci. Instr. 25, 360 (1954).
12. V. G. Levich, Physicochemical Hydrodynamics (Prentice Hall, Inc., Englewood Cliffs, N.J.), 1962.
13. A. B. Metzner and J. S. Taylor, A. I. Ch. E. J. 6, 109 (1960).
14. Y. Oyama and S. Aiba, J. Sci. Res. Inst. (Tokyo) 46, 211 (1952); Y. Oyama and K. Endoh, Kagaku Kogaku [Chem. Eng. (Japan)] 19, 2 (1955).
15. D. H. Phillips and M. V. Johnson, Ind. Eng. Chem. 51, 83 (1959).
16. H. E. Rea, Jr., and T. Vermeulen, Effect of Baffling and Impeller Geometry on Interfacial Area in Agitated Two-Phase Liquid Systems, University of California Radiation Laboratory Report UCRL-2123, April 1953.

17. W. A. Rodger, V. G. Trice, and J. H. Rushton, Chem. Eng. Progr. 52, 515 (1956).
18. J. H. Rushton, E. W. Costich, and H. J. Everett, Chem. Eng. Progr. 46, 395, 467 (1950).
19. J. S. Taylor, Flow Patterns in Agitated Vessels, M. S. thesis in Chemical Engineering, University of Delaware, Newark, Delaware, 1955.
20. J. H. Vanderveen, Coalescence and Dispersion Rates in Agitated Liquid-Liquid Systems, Lawrence Radiation Laboratory Report UCRL-8733, Dec. 1960.
21. T. Vermeulen, G. M. Williams, and G. E. Langlois, Chem. Eng. Progr. 51, 85 (1955).
22. L. H. Weiss, J. L. Fick, R. H. Houston, and T. Vermeulen, Dispersed-Phase Distribution Patterns in Liquid-Liquid Agitation, Lawrence Radiation Laboratory Report UCRL-9787, Oct. 1962.
23. K. R. Westerterp, L. L. Van Dierendonck, and J. A. De Kraa, Chem. Eng. Sci. 18, 157 (1963).
24. A. M. White, E. Brenner, G. A. Phillips, and M. S. Morrison, Trans. A. I. Ch. E. 30, 570, 585 (1934).
25. Gael M. Williams, Effect of Agitation on Interfacial Area in Unstable Gas-Liquid Emulsions (M. S. thesis in Chemical Engineering), University of California, 1954.
26. F. Yoshida, A. Ikeda, S. Imakawa, and Y. Miura, Ind. Eng. Chem. 52, 435 (1960).